NASA/TP—1999-208692

Secondary Electron Emission Spectroscopy of Diamond Surfaces

Isay L. Krainsky and Vladimir M. Asnin
Glenn Research Center, Cleveland, Ohio

Andre G. Petukhov
South Dakota School of Mines and Technology, Rapid City, South Dakota

October 1999

The NASA STI Program Office . . . in Profile

Since its founding, NASA has been dedicated to the advancement of aeronautics and space science. The NASA Scientific and Technical Information (STI) Program Office plays a key part in helping NASA maintain this important role.

The NASA STI Program Office is operated by Langley Research Center, the Lead Center for NASA's scientific and technical information. The NASA STI Program Office provides access to the NASA STI Database, the largest collection of aeronautical and space science STI in the world. The Program Office is also NASA's institutional mechanism for disseminating the results of its research and development activities. These results are published by NASA in the NASA STI Report Series, which includes the following report types:

- TECHNICAL PUBLICATION. Reports of completed research or a major significant phase of research that present the results of NASA programs and include extensive data or theoretical analysis. Includes compilations of significant scientific and technical data and information deemed to be of continuing reference value. NASA's counterpart of peer-reviewed formal professional papers but has less stringent limitations on manuscript length and extent of graphic presentations.

- TECHNICAL MEMORANDUM. Scientific and technical findings that are preliminary or of specialized interest, e.g., quick release reports, working papers, and bibliographies that contain minimal annotation. Does not contain extensive analysis.

- CONTRACTOR REPORT. Scientific and technical findings by NASA-sponsored contractors and grantees.

- CONFERENCE PUBLICATION. Collected papers from scientific and technical conferences, symposia, seminars, or other meetings sponsored or cosponsored by NASA.

- SPECIAL PUBLICATION. Scientific, technical, or historical information from NASA programs, projects, and missions, often concerned with subjects having substantial public interest.

- TECHNICAL TRANSLATION. English-language translations of foreign scientific and technical material pertinent to NASA's mission.

Specialized services that complement the STI Program Office's diverse offerings include creating custom thesauri, building customized data bases, organizing and publishing research results . . . even providing videos.

For more information about the NASA STI Program Office, see the following:

- Access the NASA STI Program Home Page at ***http://www.sti.nasa.gov***

- E-mail your question via the Internet to help@sti.nasa.gov

- Fax your question to the NASA Access Help Desk at (301) 621-0134

- Telephone the NASA Access Help Desk at (301) 621-0390

- Write to:
  NASA Access Help Desk
  NASA Center for AeroSpace Information
  7121 Standard Drive
  Hanover, MD 21076

NASA/TP—1999-208692

Secondary Electron Emission Spectroscopy of Diamond Surfaces

Isay L. Krainsky and Vladimir M. Asnin
Glenn Research Center, Cleveland, Ohio

Andre G. Petukhov
South Dakota School of Mines and Technology, Rapid City, South Dakota

National Aeronautics and
Space Administration

Glenn Research Center

October 1999

Acknowledgments

The authors wish to express their appreciation to co-workers James A. Dayton, Jr., G. T. Mearini, M. Foygel, and H. Sun, who contributed to the project at various stages of the investigation. The authors also would like to thank Stephen V. Pepper for providing single-crystal diamond and Y. Wang and J. C. Angus for providing CVD diamond films.

Available from

NASA Center for Aerospace Information
7121 Standard Drive
Hanover, MD 21076
Price Code: A03

National Technical Information Service
5285 Port Royal Road
Springfield, VA 22100
Price Code: A03

Secondary Electron Emission Spectroscopy of Diamond Surfaces

Isay L. Krainsky and Vladimir M. Asnin
National Aeronautics and Space Administration
Glenn Research Center
Cleveland, Ohio 44135

Andre G. Petukhov
South Dakota School of Mines and Technology
Rapid City, South Dakota 57701-3995

Summary

This report presents the results of a secondary electron emission spectroscopy study of hydrogenated diamond surfaces for single crystals and chemical vapor-deposited polycrystalline films. One-electron calculations of Auger spectra of diamond surfaces having various hydrogen coverages are presented, the major features of the experimental spectra are explained, and a theoretical model for Auger spectra of hydrogenated diamond surfaces is proposed.

An energy shift and a change in the line shape of the carbon core-valence-valence (KVV) Auger spectra were observed for diamond surfaces after exposure to an electron beam or by annealing at temperatures higher than 950 °C. This change is related to the redistribution of the valence-band local density of states caused by hydrogen desorption from the surface.

A strong negative electron affinity (NEA) effect, which appeared as a large, narrow peak in the low-energy portion of the spectrum of the secondary electron energy distribution, was also observed on the diamond surfaces. A fine structure in this peak, which was found for the first time, reflected the energy structure of the bottom of the conduction band. Further, the breakup of the bulk excitons at the surface during secondary electron emission was attributed to one of the features of this structure.

The study demonstrated that the NEA type depends on the extent of hydrogen coverage of the diamond surface, changing from the true type for the completely hydrogenated surface to the effective type for the partially hydrogenated surface.

Introduction

During the last decade, much attention was focused on studying the fundamental properties and applications of diamond (ref. 1). It is a promising semiconductor material for novel electronic applications because of its heat conduction properties and negative electron affinity (NEA). In comparison with diamond single crystals, chemical vapor-deposited (CVD) polycrystalline diamond films have additional advantages: their fabrication is relatively easy and cheap, they can be grown with high levels of impurity doping, and consequently they can have relatively high conductivity. With these properties, diamond can be used in the design of cold cathodes and photocathodes in high-power electronics and in high-frequency and high-temperature semiconductor devices (refs. 1 and 2).

One of the remarkable properties of diamond is the negative electron affinity of its hydrogen-covered surface. It was recently demonstrated that not only diamond single crystals (refs. 3 and 4) but also hydrogenated CVD diamond films possess a strong NEA with a coefficient of secondary electron emission σ of up to 60 (refs. 5 to 7). Also, σ decreases under electron beam exposure because of the desorption of hydrogen from the diamond surface (refs. 5 to 8). This effect can be eliminated by coating the hydrogenated surface with 10- to 100-nm-thick alkali-halide (CsI, KCl, CsF, or NaCl) films. To achieve the full NEA effect, these surfaces were activated by exposing them to an electron beam, which desorbed halogen and left a thin alkali metal film at the diamond surface (ref. 7).

This report reviews results obtained from the authors' recent investigations of hydrogenated surfaces of single diamond crystals and CVD diamond films by secondary electron emission (SEE) spectroscopy, a powerful tool for studying the bulk and surface electronic structure of solids. Auger electron spectroscopy (AES) is the most popular technique in SEE spectroscopy and has been used for many years to study the diamond surface because its spectra incorporate very important information about the composition and chemical bonding of the material. During this time, a common belief was that the carbon Auger peak for diamond was not sensitive to hydrogen on the surface (refs. 3 and 4). Also, the perception was that the surface effects were completely immaterial to the interpretation of the carbon Auger peak (ref. 9). In obvious contradiction to this perception, the authors have shown that the hydrogen desorption from the surface of diamond significantly changes both the Auger carbon peak shape and its position, which shifted towards the higher energies (refs. 10 to 13). These changes were attributed to a redistribution of the surface-carbon-valence local density of states (LDOS) that were dependent upon the extent to which hydrogen covered the surface. Therefore, although hydrogen cannot be seen in AES directly, its existence on the surface is revealed as a "fingerprint" in the fine structure of the carbon AES.

Until recently, the predominant method to spectroscopically study the NEA effect has been ultraviolet photoelectron spectroscopy (UPS) (ref. 3). We have demonstrated that SEE spectroscopy of low-energy electrons is a very efficient way to study this effect (ref. 14), and we have discovered in the surface of the SEE spectrum of the NEA a fine structure that reflected the energy structure of the bottom of the diamond conduction band (ref. 15). An analysis of the fine structure provided evidence that an exciton mechanism for SEE exists (refs. 16 and 17) and that the model chosen to describe the NEA of a diamond surface depends on the hydrogen coverage (ref. 18).

Experimental Technique

Sample Description

The experiments were performed on two types of samples: natural single-crystal diamond and chemical vapor-deposited (CVD) polycrystalline diamond. The single-crystal diamond plates had either a (111) or (100) surface, were 4 by 4 by 0.3 mm or 3 by 3 by 0.25 mm, and were cut from type-IIb, semi-insulating, natural single-crystal diamond that was slightly boron doped and had *p*-type conductivity. After the samples were brazed onto a tantalum plate by using a AgTi alloy, the plate was mounted on the top of a vacuum resistive heater, which was used to achieve sample temperatures of up to 1000 °C. Temperature monitoring was done with infrared two-color pyrometers.

The chemical vapor-deposited diamond polycrystalline films were grown on molybdenum substrates by microwave plasma CVD and were heavily doped with boron ($N_A \approx 10^{18}$ to 10^{19} cm^{-3} as estimated from the film conductivity measurements). Raman spectroscopy of the grown CVD films showed a negligible background of nondiamond carbon and a very sharp peak at 1331 cm^{-1}, characteristic of the diamond sp^3 bond. After deposition, the diamond films were exposed to air, and only carbon was observed in their Auger spectra. The film thickness ranged from 10 to 20 μm.

The sample surfaces were prepared by employing the standard techniques for diamond (ref. 19): mechanical polishing by using 0.25-μm-grit diamond paste and olive or lapping oil as a paste extender, followed by cleaning in an ultrasonic bath with acetone and alcohol. Although a prevalent opinion holds that the olive oil is a source of hydrogen for the diamond surface (ref. 20), the authors did not observe that any of the surface properties were dependent on the polishing oil.

The heater containing the samples was mounted on an XYZ-manipulator and positioned at the center of an ultrahigh-vacuum chamber (base pressure of 1×10^{-10} torr, fig. 1). Before the measurements, the single-crystal samples were annealed at 500 °C for 30 min.

Decreasing the hydrogen coverage of the diamond surfaces was achieved by exposing them to the cylindrical mirror energy analyzer (CMA) electron gun beam and annealing at temperatures higher than 950 °C.

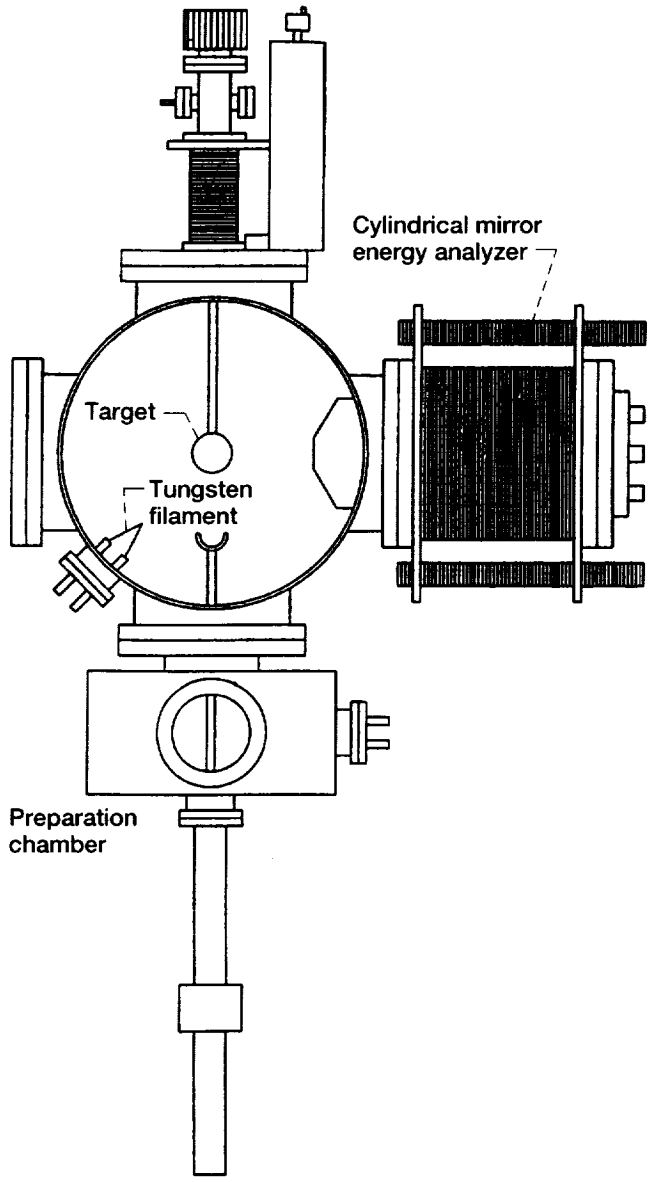

Figure 1.—Experimental setup.

The single-crystal diamond surface was rehydrogenated by room-temperature exposure to atomic hydrogen produced from the molecular hydrogen background by a hot tungsten filament heated to temperatures of about 1900 °C. Coverage saturation was observed after a 30-min exposure at a hydrogen pressure of 1×10^{-5} torr. For as-received CVD diamond films, the same exposure to molecular hydrogen was sufficient to restore the hydrogen coverage (refs. 5 to 7, 11, and 14). However, for annealed or treated diamond CVD films and the single-crystal surfaces, rehydrogenation was possible only by exposure to atomic hydrogen.

Measurement Technique

Measurements of electron energy spectra.—The energy spectra of the secondary electrons were measured by a single-pass (Perkin-Elmer) CMA having a 0.6-percent energy resolution and a 42±6° collection angle. Although monitoring the electron energy spectra of highly doped CVD diamond films was a routine procedure and could be done in the dc mode, taking electron spectra of the semi-insulating natural diamond crystal was a much more complicated procedure because of sample charging. To prevent charging that usually distorts the electron spectra, we combined the pulse method of measurement with sample heating (ref. 21), which prevented charge accumulation and increased charge dissipation.

The pulsed primary current was created by applying to the Wehnelt of the CMA electron gun a sum of negative turn-off dc bias voltage and positive rectangular turn-on pulses from a pulse generator (fig. 2, trace 1). To monitor sample charging, the secondary electron current pulses were amplified and observed on an oscilloscope. When surface charging occurred, we observed the pulse decaying, or losing its rectangular shape and amplitude. To prevent this occurrence, the proper combination of pulse duration and frequency, sample temperature, and primary current density were selected for each measurement. At room temperature, the measurements showed that

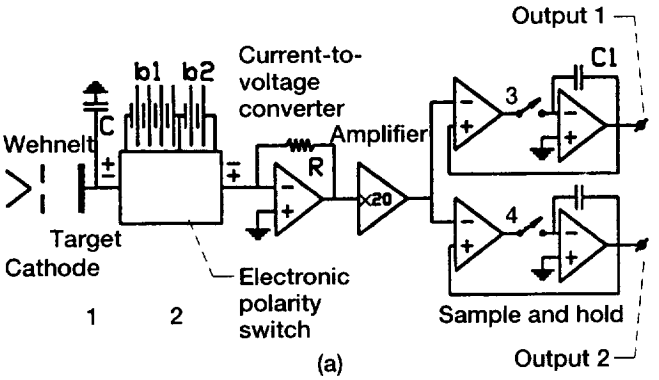

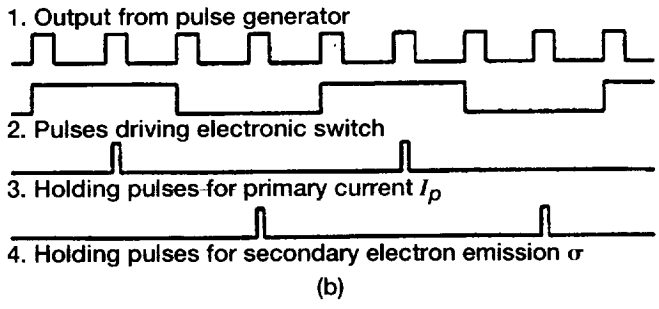

Figure 2.—Measurements of SEE properties in pulse mode. (a) Block diagram of pulse measurements of SEE coefficent. (b) Timing diagram of various voltages supplied to (a).

the charging occurred at pulse durations longer than 3×10^{-7} s, frequencies higher than 1 kHz, and primary current densities from 10^{-5} to 10^{-4} A/cm^{-2}. Increasing the sample temperature to 400 to 500 °C allowed the use of significantly longer pulses (up to 10^{-5} s) and higher frequencies (up to 5 kHz), thereby improving the data collection time and the signal-to-noise ratio. Changing these pulse parameters by a factor of 2 to 4 did not affect the measured energy position and shape of the secondary electron spectrum within the instrumentation accuracy of about 0.1 eV.

To avoid the creation of an additional unknown bias of the sample relative to the ground (the effect of current flowing along the resistive heater), the sample was heated in a pulsed mode. Secondary electrons were detected only during the intervals between the heating current pulses. The computer controlled the width and the period of the heating current pulses, set at 1 and 2 s, respectively. These times were at least 1 order of magnitude smaller than the time required for the sample temperature to stabilize.

The absence of the artifact of charging was proven by measuring a shift in the onset of the secondary electrons when small negative potentials (0.5 to 5 eV) were applied to the target (ref. 14). The target bias was used to compensate for the work function difference between the target and the analyzer and to make the measurements of the very low-energy region of the spectrum reliable. In this range of the applied bias in the absence of charging, the measured electron spectra shifted linearly with the voltage. The energy of secondary electrons in the spectra of low-energy electrons was measured with respect to the Fermi level of the sample. The position of the Fermi level was determined from the location of the σ-peak in the secondary electron spectra of a graphite sample, Aquadag (ref. 22).

The data were collected by counting electron pulses from an electron multiplier, filtered, differentiated, and filtered again to obtain standard Auger spectra.

Pulsed measurements of SEE coefficient.—Surface charging of semi-insulating and insulating crystals even at extremely low primary currents makes it impossible to use the traditional dc method of measuring the SEE coefficient σ. This effect causes redistribution of the secondary and primary electron currents and results in a measured value of $\sigma \cong 1$. Johnson (ref. 23) was probably the first who measured σ by irradiating the target with short electron pulses and observed the pulses that were proportional to the secondary and primary currents on an oscilloscope screen. We designed the device to measure σ by utilizing sample-and-hold amplifiers and electronic switching of the target potential (ref. 24). This device (fig. 2(a)) allowed us to simultaneously monitor both σ and the primary current for an insulating sample and to record the data using a computer.

The primary (secondary) electron current was measured by using an electronic switch (fig. 2(a)) to apply a negative (positive) potential of up to 100 V to the target. The switch was driven by a square pulse (trace 2 of fig. 2(b)), and the highs and lows of the pulse corresponded to a positive or negative potential,

respectively, applied to the target. The current pulses were converted to voltage pulses, were amplified, and were sent to the two high-speed bipolar sample-and-hold amplifiers. The short "holding" pulses (traces 3 and 4 in fig. 2(b)) with adjustable pulse width and delay were applied so that we could measure the signal pulse amplitude with either positive or negative voltage applied to the target. When doing so, the upper sample-and-hold amplifier in figure 2(a) was holding the voltage V_1 proportional to the primary current I_p and the lower sample-and-hold amplifier was holding the voltage V_2 proportional to the secondary current I_2. The output voltages were filtered, digitized, and read by a computer that produced and plotted both $\sigma = 1 - V_1/V_2$ and primary current I_p versus the energy of the primary electrons.

Auger Spectroscopy of Diamond Surfaces

An Auger core-valence-valence (KVV) process involves a three-particle interaction of two valence electrons and a core hole in the initial state and two valence holes and an Auger electron in the final state. The kinetic energy of the free Auger electron, which escapes the solid, is measured experimentally. It is evident that the Auger line shape is related to both the local density of states (LDOS) of the valence band and the matrix elements of the Coulomb interaction between wave functions of the initial and final states (refs. 25 to 27).

The typical Auger spectrum of a clean diamond surface (fig. 3) consists of carbon peaks only. Comprising this spectrum are the main peak A_0 and its satellites A_1, A_2, A_3. The energy of Auger electrons in diamond is within the range of 240 to 280 eV and their mean free path does not exceed a few interatomic distances (ref. 28). This means that the contribution of the surface density of states to the total density of states cannot be ignored. However, as mentioned in the Introduction, there is a perception (ref. 9) that the surface effects are not important in the interpretation of the carbon KVV Auger spectra. From this viewpoint, the presence of foreign atoms chemically bound to the surface should not affect the KVV Auger line shapes of the host atoms. In contradiction, the studies presented herein have shown that the hydrogen desorption from the diamond surface significantly changes both the Auger carbon peak position (which shifted towards the higher energies) and its width. These changes were explained as the redistribution of the surface carbon valence LDOS, which was dependent on the extent that hydrogen covered the surface.

Experimental Results

Figures 4 and 5 demonstrate the carbon A_0 (KV_1V_1) Auger peak for single-crystal diamond with (111) and (100) surfaces, respectively, measured before and after surface exposure to the primary electron beam at various fluences (total amount of charge per unit area deposited on the surface). One can see that

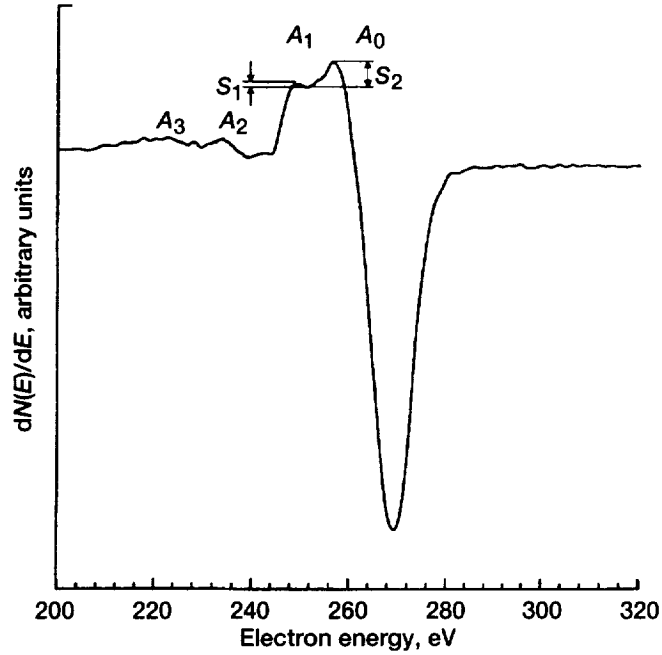

Figure 3.—Auger spectrum of carbon for clean diamond surface. Main peak, A_0; satellite peaks, A_1 to A_3; low-energy peak amplitude, S_1; high-energy peak amplitude, S_2.

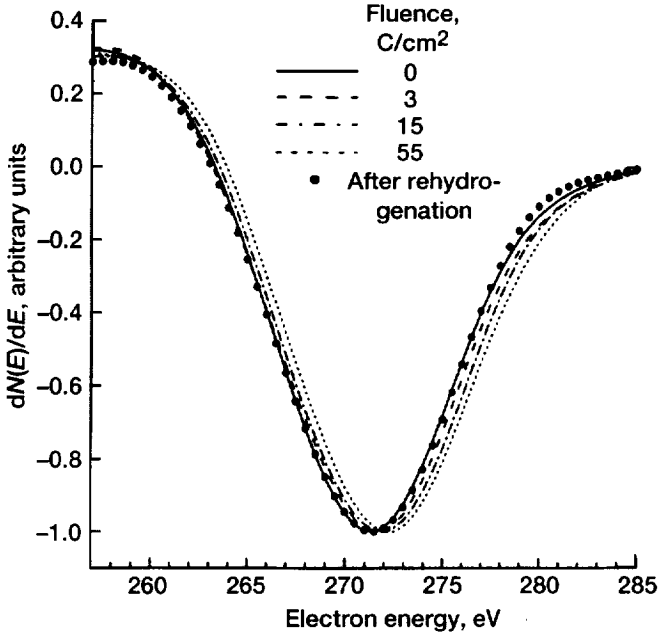

Figure 4.—Carbon Auger peak A_0 for (111) single-crystal diamond surface after various electron beam exposures and subsequent rehydrogenation.

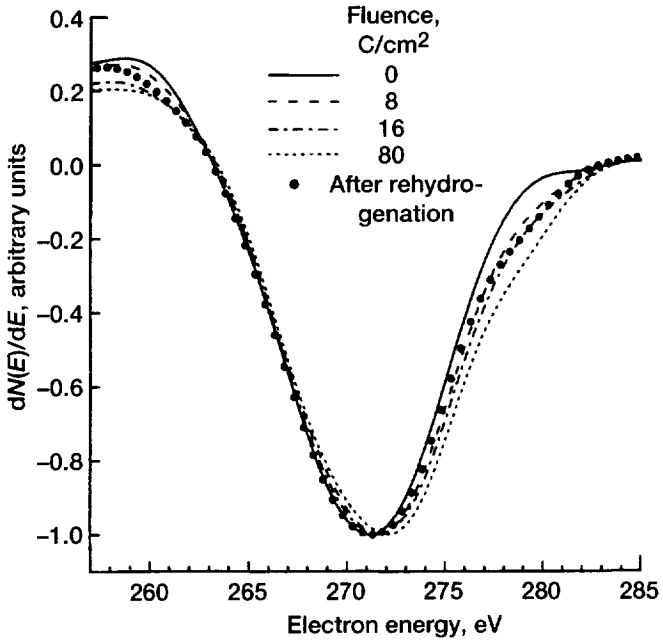

Figure 5.—Carbon Auger peak A_0 for (100) single-crystal diamond surface after various electron beam exposures and subsequent rehydrogenation.

the exposure of the surface resulted in both the shift of the peak position towards higher electron energies and the increase in its full width at half maximum (FWHM). Both changes leveled off with the increase in exposure reaching the values of about 1 eV for the shift and 0.4 to 0.8 eV for the change in the FWHM.

Corresponding changes in A_1 (KV_2V_2) features located at the low-energy side of the main A_0 peak are shown in figures 6 and 7 for the (111) and (100) surfaces, respectively. The electron beam exposure caused the ratio of the low-energy peak amplitude S_1 to the high-energy peak amplitude S_2 to increase, as observed earlier (ref. 8). As seen from the figures, this phenomenon was more pronounced for the (100) diamond surface.

The same phenomenon was observed after annealing the sample at temperatures higher than 950 °C when hydrogen is well known to desorb from the diamond surface (ref. 20). The Auger peak A_0 of the crystal surface before and after annealing are displayed in figure 8. The change in the satellite structure after annealing was well documented by Pate (ref. 20).

Exposure of the diamond surface to the primary electron beam and to annealing at $T \geq 950$ °C results in the desorption of hydrogen (refs. 8 and 20) and in the decrease in secondary electron yield σ of the diamond (refs. 5 to 7). In addition to AES of the single crystal, we monitored σ (in the pulse mode to avoid the charging effect) and found that the changes in the Auger spectra after electron beam exposure and annealing were accompanied by a sharp decrease in σ_{max} from the initial value of about 70 to about 1 (fig. 9). The high value of σ is a consequence of the strong negative electron affinity specific to the hydrogen-covered diamond surface (refs. 3, 20, 29, and 30).

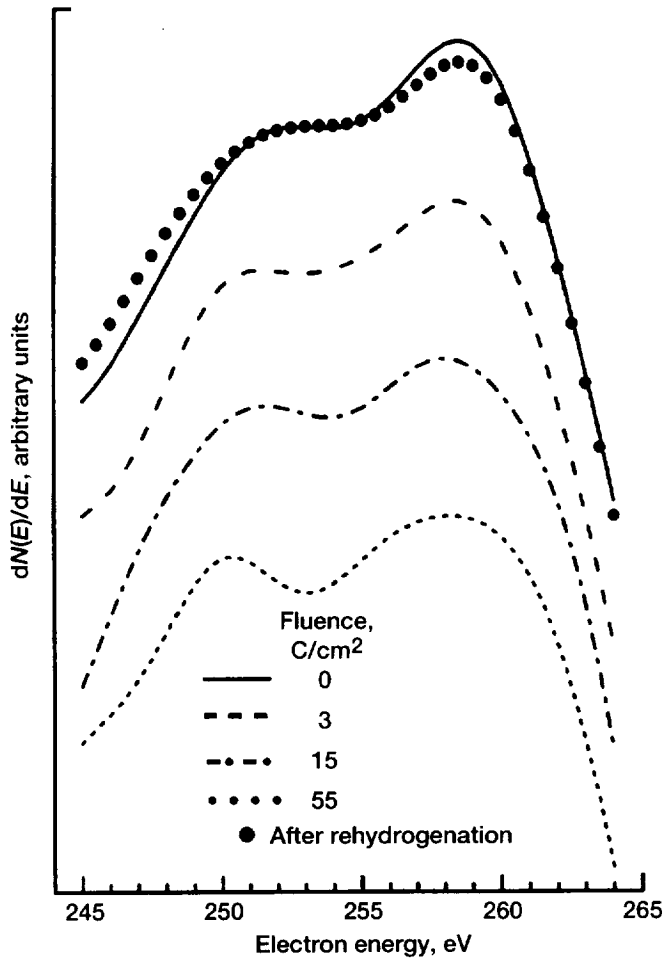

Figure 6.—Fine structure of A_1 feature for (111) single-crystal diamond surface after various electron beam exposures and subsequent rehydrogenation.

All the phenomena described above for the single-crystal diamond surfaces were also observed for the diamond CVD films. Figure 10 presents the results of measurements of the A_0 Auger peak position and its FWHM as a function of electron beam exposure for an as-received CVD diamond film. The data were obtained when these parameters were monitored during continuous beam exposure and were plotted as a function of fluence. As seen in this figure, an increase of up to 1.2 eV in energy and of about 0.2 eV in FWHM were observed for a polycrystalline diamond film. Figure 11 demonstrates the change in the S_1/S_2 ratio in the A_1 feature of Auger spectra (see fig. 3) and in σ for the CVD diamond film as a function of the fluence. The increase in fluence results in a simultaneous increase in the S_1/S_2 ratio and a decrease in σ_{max}.

All the observed changes for the single-crystal diamond surfaces and the CVD diamond films were reversible after rehydrogenation, which restored the initial position of the Auger peak, its shape (including the fine structure), and the value of σ (figs. 4 to 7 and 12). Therefore, we can conclude that these

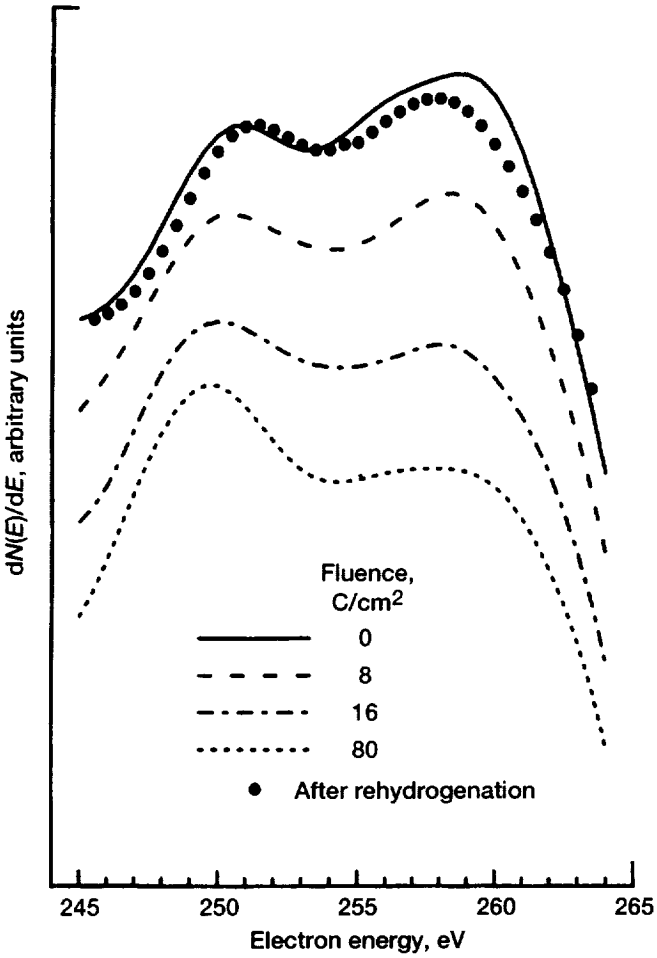

Figure 7.—Fine structure of A_1 feature for (100) single-crystal diamond surface after various electron beam exposures and subsequent rehydrogenation.

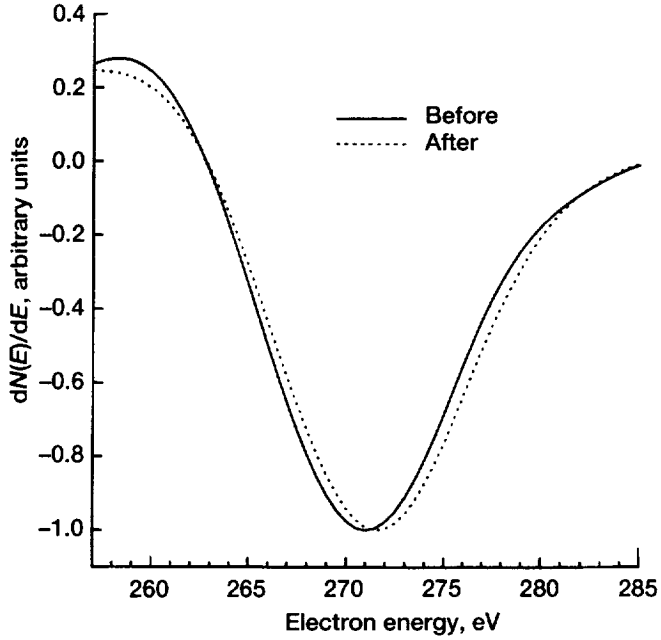

Figure 8.—Carbon A_0 Auger peak for single-crystal diamond before and after annealing at 950 °C.

changes in the diamond Auger spectrum were directly related to the extent that hydrogen covered the diamond surface.

Computational Procedure

The basic KVV Auger process is described as follows. A valence-band electron is captured by a previously created core-hole state c. The energy of recombination is transferred to another nearby valence electron, providing it the energy to leave the crystal. As a result, two holes (k and l) in the valence band are generated. The energies of these holes lie in the continuous spectrum of the valence band. Therefore, the kinetic energy of the ejected Auger electron E_A is expressed as

$$E_A = I_c - (I_k + I_l + U_{\text{eff}}) \tag{1}$$

where $I_{c,k,l}$ are the ionization energies of the corresponding electronic states relative to the vacuum level and U_{eff} is the effective Coulomb energy of interaction between the two valence holes in the final state (refs. 31 and 32). To calculate the energy distribution of the Auger electrons, the probability of the elementary process should be integrated over the ionization energies I_k and I_l of the valence-band holes.

This paragraph describes a typical procedure for the calculation of the KVV Auger spectrum for diamond or graphite (refs. 33 and 34). The local densities of states (LDOS) of the valence s- and p-electrons, which are either evaluated theoretically or extracted from photoemission measurements, are used to calculate different convolutions of partial LDOS (s-s, s-p, and p-p) weighted with the corresponding matrix elements of Coulomb interaction. At the end, these convolutions are added to calculate the Auger electron distribution. The Coulomb matrix elements are usually taken from the atomic calculations whereas the hole-hole partial effective interaction energies U^{ss}_{eff}, U^{sp}_{eff}, and U^{pp}_{eff} (ref. 33) serve as fitting parameters. This procedure gives a reasonably accurate description of experimental data for graphite (ref. 33), laser-deposited a-C, a-C:H, and single-crystal diamond (ref. 34).

This calculation procedure usually employs a large number of parameters to fit the experimental data. Furthermore, it is usually based only on bulk LDOS and underestimates the influence of the surface, which is expected to be very important for Auger spectra calculations, particularly with an adsorbate present.

The effects of the hydrogen adsorption on the Auger spectrum of the diamond surface were analyzed by using the first-principle, local density approximation (LDA) method (refs. 35 and 36) for the calculations of the LDOS and Auger matrix elements. The surface and core-hole effects were taken into

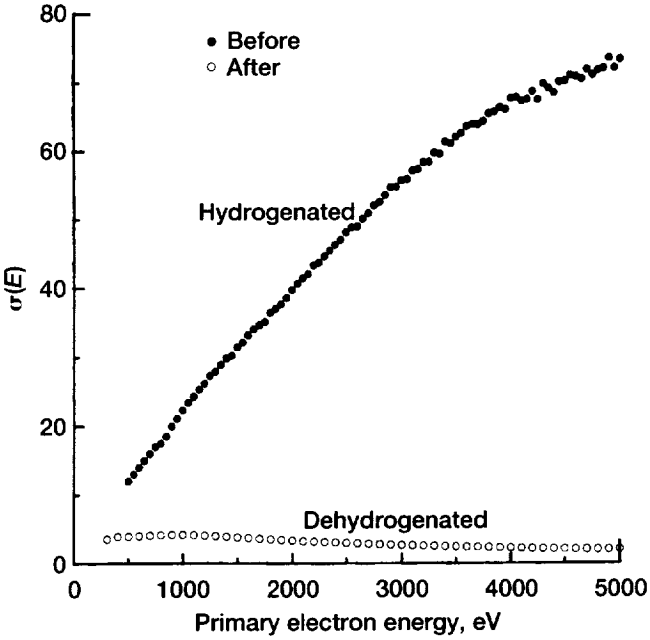

Figure 9.—Secondary electron yield σ for hydrogenated single-crystal diamond suface before and after annealing at 950 °C.

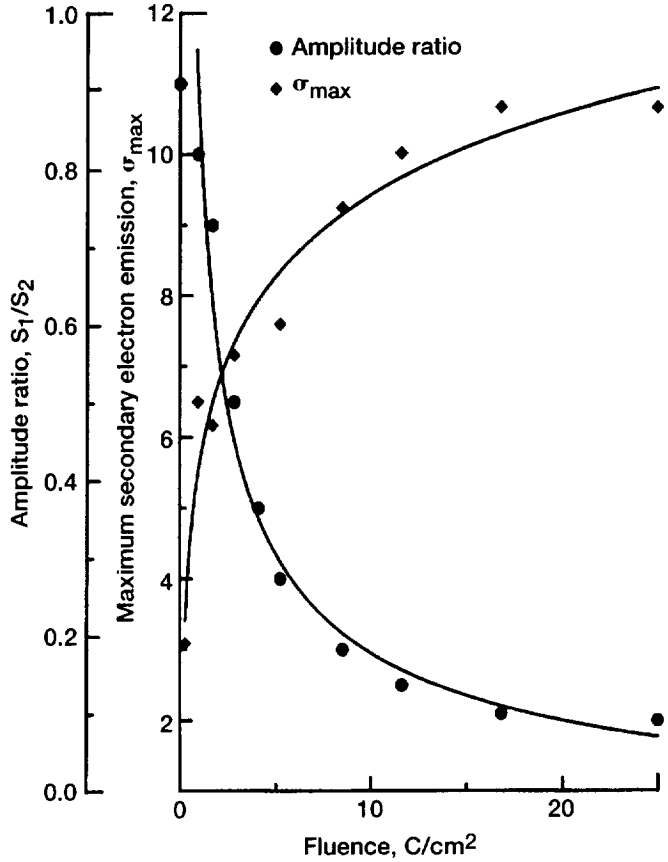

Figure 11.—Ratio S_1/S_2 of fine structure amplitudes for A_1 feature of Auger spectra and σ_{max} as function of fluence for CVD diamond film.

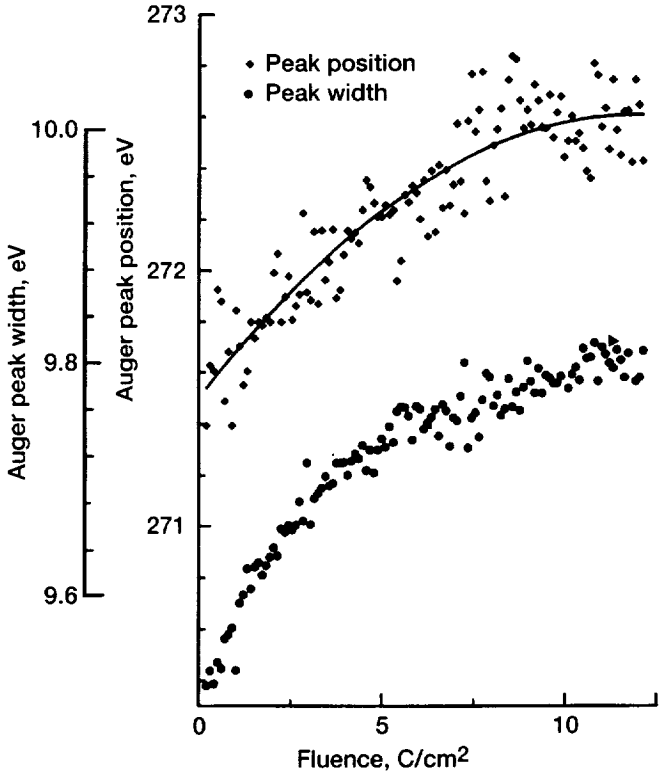

Figure 10.—Auger peak A_0 position and full width at half maximum (FWHM) as function of fluence for as-received chemically vapor-deposited (CVD) diamond film.

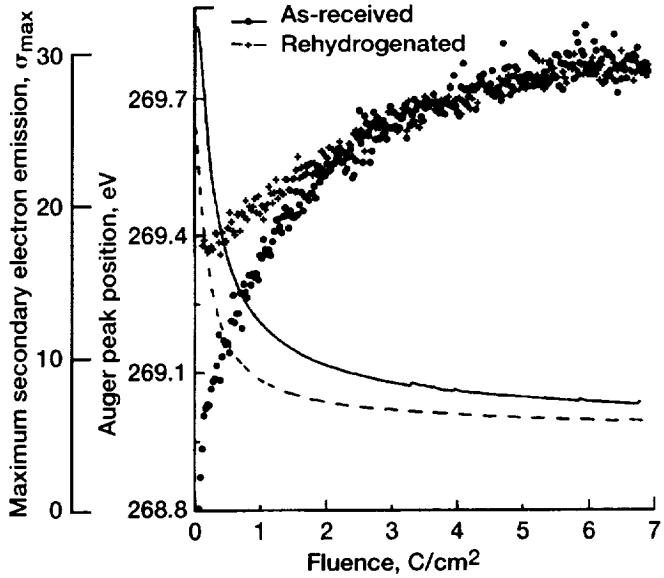

Figure 12.—Dependence of Auger peak A_0 position and σ_{max} on fluence for CVD diamond film.

account; however, we did not introduce any fitting parameters because our intent was to give a correct semiquantitative description of the experiment and not to expect our results to describe the experimental data perfectly.

While calculating the Auger spectrum $N(E_A)$, we adopted a simplified version of the theory of the KVV processes developed by Almbladh, Morales, and Grossmann (refs. 37 and 38). We considered the wave functions of the valence electrons involved in the basic Auger process to be atomiclike, linear, muffin-tin orbitals (LMTO). These orbitals belong to the same atom as the core hole (refs. 25 to 27, 31, 32, 37, and 38) and are therefore perturbed by the core hole, an occurrence usually referred to as a static core-hole effect (ref. 33). Inside the crystal, the wave function of the ejected Auger electron incorporates an exponentially decaying factor $\exp(-\lambda|z_j|/2)$, where $1/\lambda$ is a typical escape length (in our case is of the order of 10 Å) and $|z_j|$ is a distance of the j^{th} atomic plane from the surface. It is possible to show that (see also refs. 25 to 27, 37, and 38)

$$N(E_A) = 2\pi \sum_j \exp\left(-\lambda|z_j|\right) N_j(E_A) \tag{2}$$

where

$$N_j(E_A) = \sum_{l,l'} \int_{VB} M_{ll'}(E_A - I_c, E)$$

$$\times n_l^j(E_A - I_c - E) n_{l'}^j(E)\mathrm{d}E \tag{3}$$

In equations (2) and (3), j enumerates atomic layers; $l = 0,1$ (s,p) are orbital momentum quantum numbers; n_l^j is the partial local densities of states, and

$$M_{ll'} = \left(\frac{\sqrt{2E_A}}{8\pi^3}\right) \sum_{k,l_A} \frac{2}{2k+1} \begin{pmatrix} l\, l_c\, k \\ 0\ 0\ 0 \end{pmatrix}^2$$

$$\times \begin{pmatrix} l'\, l_A\, k \\ 0\ 0\ 0 \end{pmatrix}^2 \left|R_k(l,l',l_c,l_A)\right|^2 \tag{4}$$

are the matrix elements of the Coulomb interaction between the wave functions of the initial and final states.

The matrix elements in equation (4) are expressed through Wigner 3j-symbols and Slater radial integrals $R_k(l,l',l_c,l_A)$ (ref. 39) with l_c being an orbital quantum number of the core hole (for the 1-s carbon core state, $l_c = 0$); l, l', and k are the orbital quantum numbers of the valence electrons, and l_A is an orbital number of the Auger electron partial wave. In equations (2) and (3), functions $N_j(E_A)$ describe the contributions to the Auger spectra from the subsequent layers. The partial LDO n_l^j represents the outputs of the self-consistent LMTO calculations. The matrix elements can also be calculated if the radial parts of the self-consistent LMT orbitals are known. In equation (4), we assume that the wave functions of valence electrons and the partial LDOS are both perturbed by the 1-s core hole localized on a carbon atom.

To model partially hydrogenated (111) and (100) diamond surfaces, we used respectively 8- and 10-layer symmetric diamond slabs. First-principle LDA-LMTO calculations in the atomic sphere approximation (ASA, ref. 40) were performed for these slabs, both sides of which had one monolayer of hydrogen atoms. For both (100) and (111), all dangling bonds (one bond per carbon atom for the (111) surface and two bonds per carbon atom for the (100) surface) were passivated with hydrogen. Five empty spheres between periodically repeated slabs were introduced to simulate a vacuum.

We performed a series of self-consistent slab calculations of the electronic structure for different depths z_j of the core-hole layer with respect to the surface. Consequently, we calculated functions $N_j(E_A)$ with various layer numbers j, where $j = 1$ corresponds to the surface layer and $j = 4$ or 5 corresponds to the central (bulklike) layer of the (111) or (100) slab, respectively.

The effect of the fractional hydrogen coverage of the diamond surface was modeled by introducing a fractional effective atomic number ($0 \le A \le 1$) for the surface hydrogen atoms, with $A = 1$ corresponding to a 100-percent coverage and $A = 0$ corresponding

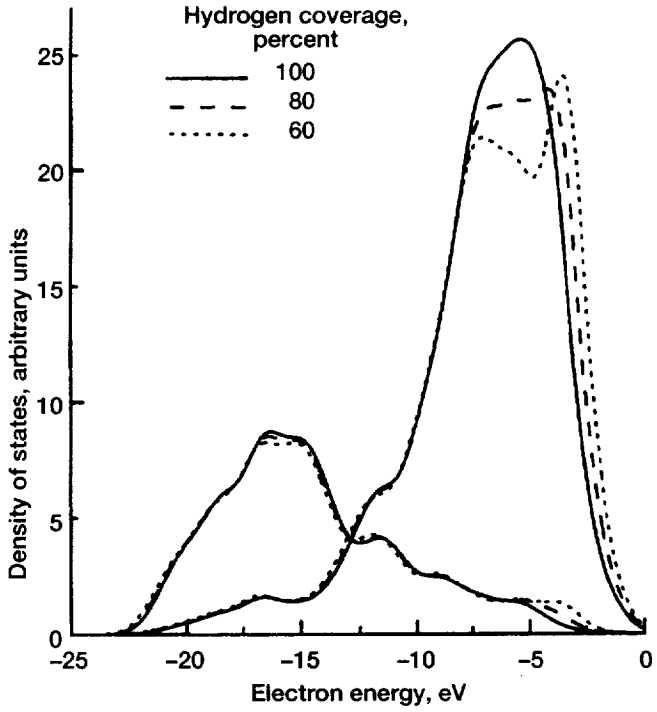

Figure 13.—Valance s- and p-electrons partial local density of states (LDOS) for (111) surface carbon atoms (with static core-hole effects taken into account) for various hydrogen coverages.

to a "clean" unreconstructed diamond surface. A half-width parameter equal to 0.08 Ry was introduced to assure sufficient smoothness of the final Auger spectra and their derivatives.

Discussion

Figure 13 displays the surface LDOS for the (111) diamond surface with different hydrogen coverages. The calculations showed that the C-H bond gives its main contribution to the LDOS in the area of the higher energy (p-type) peak. Therefore, the removal of hydrogen would affect the density of states mostly in this region (fig. 13). At coverages less than 80 percent, the figure displays a separate C-H peak splitting and shifting towards the band gap.

Figures 14(a) and 15(a) show the effects of hydrogen coverage on the calculated KVV Auger line of diamond. It is clearly seen that hydrogen desorption causes this spectrum to shift towards higher kinetic energies and to broaden slightly. These effects are due to changes in the partial LDOS for the p-states displayed in figure 13 for the (111) surface.

The changes in the derivatives of the Auger spectra calculated for different hydrogen coverages appear to be more noticeable (figs. 14(b) and 15(b)). The removal of hydrogen has the strongest effect on the position and the shape of the main minimum A_0, as just mentioned. It also can be seen that the low-energy fine structure A_1 is affected.

Our calculations are in agreement with the fact (well-established for diamond) that the fine structure of the low-energy region of the Auger spectra is determined by all the partial convolutions (s-s, s-p, and p-p) of the valence-band states. It is clearly seen from figures 14(b) and 15(b) that the relative intensities of the different fine structure maximums depend on the surface orientation and the hydrogen coverage.

The results of the calculations qualitatively agree with the observed behavior of the carbon Auger peak during hydrogen desorption from the diamond surface. A comparison of the experimental data from figures 4 to 12 and the theoretical calculations from figures 14(b) and 15(b) shows that the calculations give the right qualitative description of the Auger peak shifting towards high energies and its becoming broader. Also concluded from these figures is that the changes in the patterns of the fine structure are correctly described by our theoretical model. Note, however, that our calculations did not take into account the surface lattice reconstruction that occurs at low

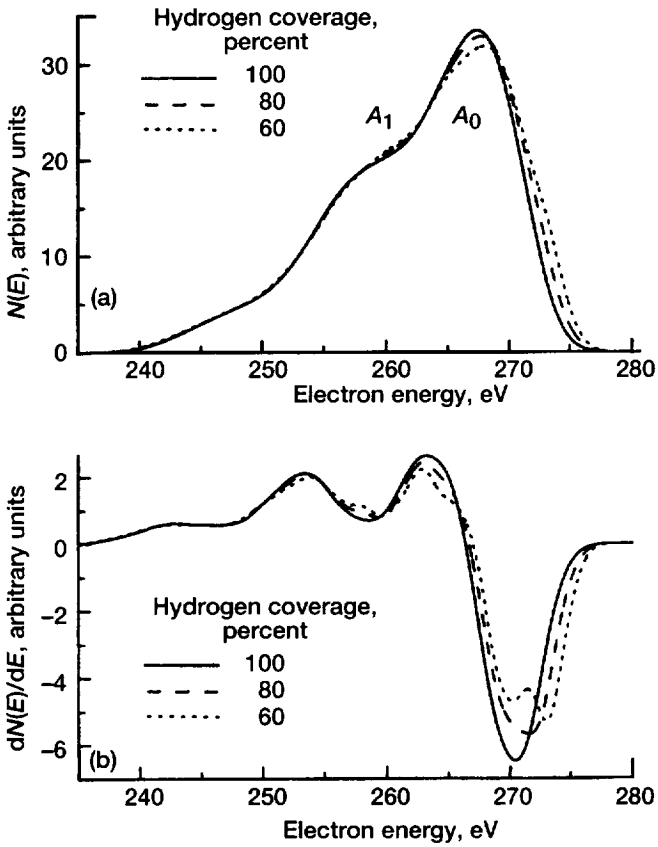

Figure 14.—Effects of hydrogen coverage on calculated KVV Auger line of diamond (111) surface. Auger spectrum (a) and its derivative (b) of (111) diamond surface for various hydrogen coverages.

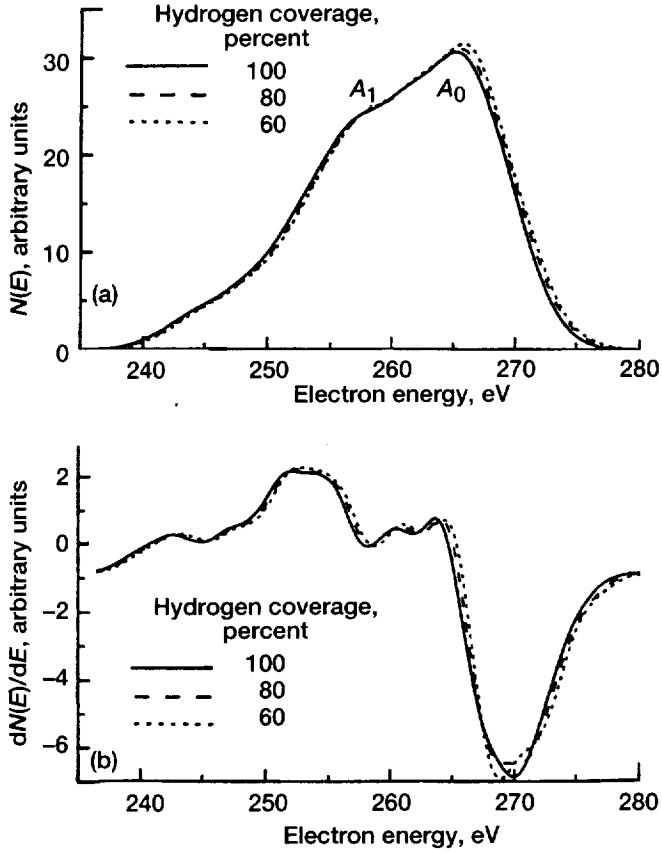

Figure 15.—Effects of hydrogen coverage on calculated KVV Auger line of diamond (111) surface. Auger spectrum (a) and its derivative (b) of (100) diamond surface for various hydrogen coverages.

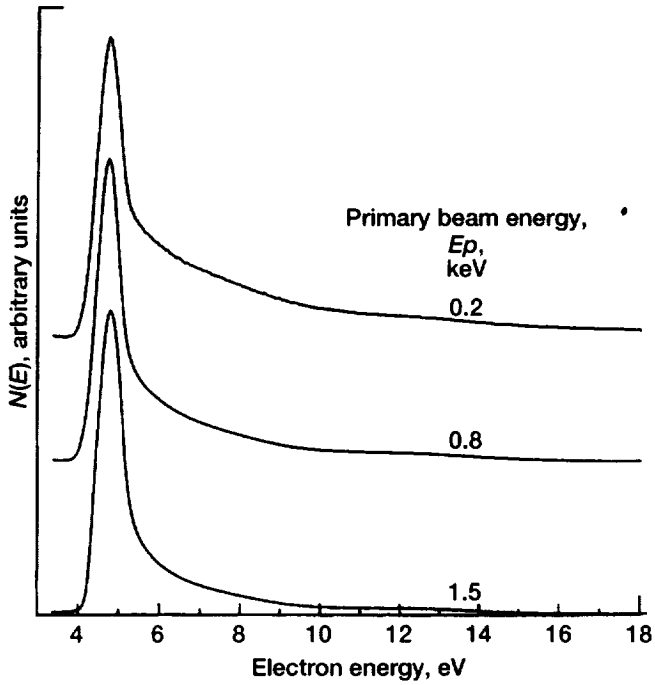

Figure 16.—Secondary electron energy distributions for diamond CVD film at bias V_t of −1.5 V and various primary beam energies. Curves are normalized to low-energy peak maximum.

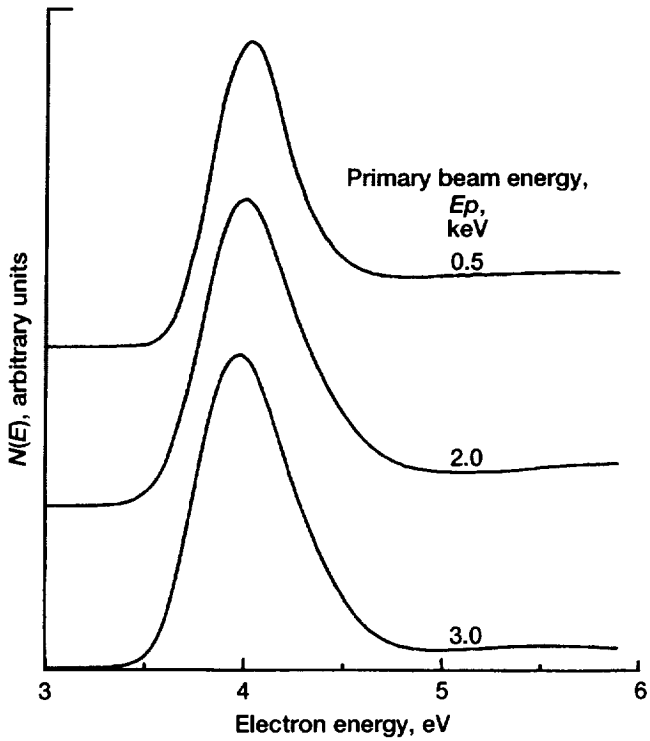

Figure 17.—Energy distributions of secondary electrons for single-crystal diamond at bias V_t of −1.5 V and various primary beam energies. Curves are normalized to low-energy peak maximum.

hydrogen coverages of the diamond surface (ref. 20). For example, for the (111) surface, this reconstruction resulted in the appearance of a DOS peak at 1.1 eV below the top of the valence band (ref. 20) that can probably limit the value of the Auger peak shift and the change in its width. Neglecting the surface reconstruction might also be the reason for the appearance of the artificial splitting of the A_0 peak in the theoretical Auger spectrum (figs. 14 and 15) that was not observed experimentally.

Negative Electron Affinity of Diamond Surfaces

Study of Negative Electron Affinity by Secondary Electron Emission Spectroscopy

A semiconductor surface has the property of NEA when the vacuum energy level lies below the absolute minimum of the conduction band and allows electrons to escape into the vacuum without being reflected by a potential barrier (ref. 41). These electrons appear in the UPS spectrum as a very high-intensity, narrow peak at a low electron energy (ref. 3). The NEA phenomenon has been studied in diamond because it promises to be a good semiconductor material for electronic applications. As mentioned in the Introduction, the prevalent method used for these studies has been ultraviolet photoelectron spectroscopy (UPS); however, in the present study, we used SEE spectroscopy because we expected to see a similar peak at the low-energy edge of the SEE spectra when the NEA surface was bombarded with a beam of primary electrons. The origin of this peak is explained as follows. Hot electrons, excited by the primary beam to the conduction band, lose their energy as a result of electron-electron and electron-phonon interactions and accumulate at the bottom of the conduction band. At an NEA surface, these electrons can be emitted into the vacuum without being reflected by a potential barrier and appear in the UPS spectra as a very intensive and narrow peak at a low electron energy.

Figures 16 and 17 show the low-energy portion of the secondary electron spectra of an as-grown CVD diamond polycrystalline film and a single-crystal diamond at various primary beam energies E_p. Note that most of the secondary electrons are collected in the form of the narrow low-energy peak with the FWHM ranging from 0.5 to 0.6 eV. After measuring the energy distributions for various primary energies, we found that the contribution of this peak to the total number of the measured secondary electrons increases with an increase in the primary energy. The ratio K of the number of low-energy electrons in this peak (the area under the peak) to the total number of the measured true secondary electrons with an energy less than 14 eV (the corresponding area under the distribution

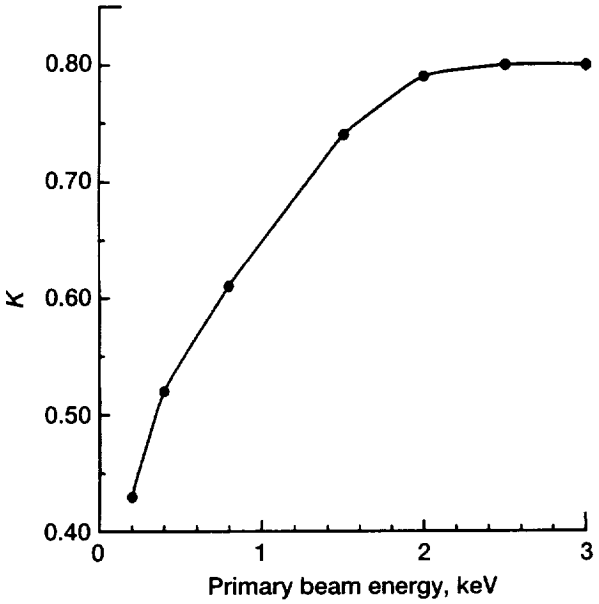

Figure 18.—Ratio K of number of electrons under low-energy peak in $N(E)$ to total number of observed secondary electrons as function of primary energy for diamond CVD film.

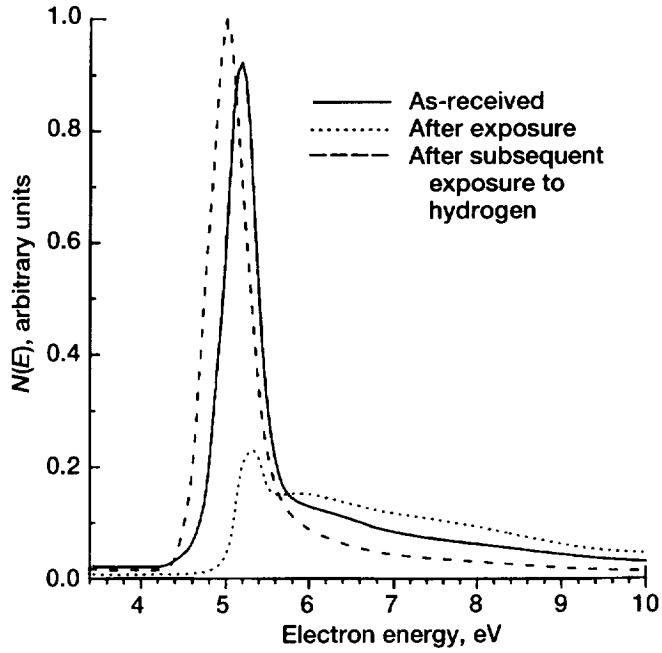

Figure 19.—Energy distributions of secondary electrons for as-grown CVD diamond film after exposure to electron beam for up to 6 hr at current density of 0.18 mA/cm^2 and primary beam energy E_p of 3 keV and after subsequent exposure to molecular hydrogen environment at pressure of 5×10^{-6} torr for 1 hr. Data are normalized to low-energy peak maximum of dashed curve. V_t = –1.5 V.

curve) as a function of the primary energy E_p is shown in figure 18 for a CVD film. The behavior of this dependence is discussed later in the section Fine Structure in Secondary Electron Emission Peak of Diamond with NEA Surface.

Previously reported in references 17 and 28 and demonstrated in the Experimental Results section is that continuous irradiation of the diamond CVD films by an electron beam results in the desorption of hydrogen from the surface and in the decrease in the SEE yield. Figure 19 shows the direct correlation observed between hydrogen coverage and the NEA effect on the diamond film surface. The transformation of the secondary electron spectrum after the treatment of its surface by exposure to the electron beam for up to 6 hr at a current density of 0.180 mA/cm^2 and E_p = 3 keV led not only to a significant reduction in the value of σ (from 32 to 5 for this sample) but also to a decrease in the low-energy-peak contribution to the energy distribution (the dotted curve). Subsequent exposure of the sample to a hydrogen environment at a pressure of 5×10^{-6} torr for 30 min restored the distribution function of the secondary electrons (dashed curve) to its original form.

Origin of NEA for Diamond Surface

Two types (models) of negative electron affinity are described, the effective and the true (fig. 20). The effective NEA model is a combination of positive electron affinity and depletion band bending at the surface of the semiconductor. This band bending can cause the vacuum energy level to occur at an energy below the minimum of the conduction band (ref. 41). The magnitude of the effective NEA is determined as $\chi_{eff} = \varphi_{BB} - \chi$, where χ is positive electron affinity and φ_{BB} is band bending (fig. 20(a)). In the case of the true NEA model, χ becomes negative due to the existence of a dipole layer on the semiconductor surface, allowing the NEA effect to be observed even for flat bands near the surface. Depletion band bending in this case increases the NEA effect: $\chi_{true} = \varphi_{BB} + \chi$ (fig. 20(b)).

It has been argued that the true NEA model can be applied to the surfaces of natural crystal diamond even when band bending exists near its surface (ref. 30).

The present investigations of the secondary electron energy distribution from CVD diamond polycrystalline films showed that the type of NEA depends on the extent of surface hydrogen coverage, which changes after annealing. The CVD films used to measure the coefficient of SEE underwent multiple rehydrogenation cycles (5 to 10). Each cycle included sample annealing at temperatures higher than 950 °C (to remove hydrogen from the surfaces) and subsequent room-temperature exposure of the diamond surface to atomic hydrogen. The treated surfaces demonstrated an NEA that was uniform over the entire surface and was also reversible after rehydrogenation. These surfaces had a maximum coefficient of secondary electron emission up to 50 at a primary electron energy E_p of 3 keV.

The surface hydrogen coverage was changed by heating the sample to increasingly higher temperatures in the range of 600 to 975 °C in 10-min increments. After each heating step, the

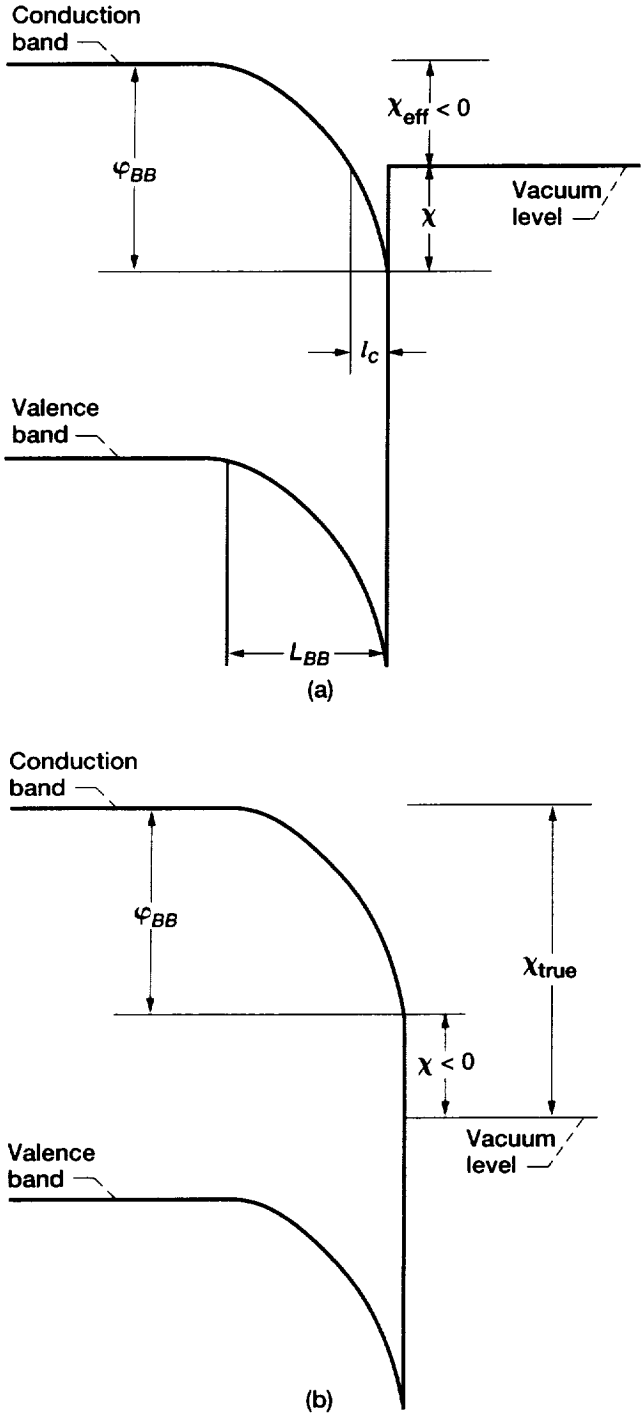

Figure 20.—Near-surface band of semiconductor for models of (a) effective negative electron affinity (NEA) and (b) true NEA.

coefficient of SEE as a function of E_p was measured using the pulse method described in the section Measurement Technique. The maximum value of $\sigma(E_p)$ was considered a relative measure of the surface hydrogen coverage.

Figure 21 presents the curves of $\sigma(E_p)$ measured after sample heating at various temperatures and shows that σ decreased monotonically when the temperature was increased from 600 to 950 °C. The effect is evidently due to gradual hydrogen desorption from the sample surface (refs. 5 to 7). In our experiments, we were not able to observe any increase in σ after the samples were heated at temperatures above 500 °C as described in reference 42.

Figure 22 demonstrates the behavior of the low-energy portion of the secondary electron energy distribution at various hydrogen coverages for a CVD diamond surface. The data in figure 22(a) were obtained immediately after the surface was saturated with hydrogen and the sample had a maximum value of $\sigma_{max} = 35$. In this case, the low-energy peak characteristic of NEA surfaces appeared even at the lowest energy of the primary electrons (10 eV) reported herein. For such primary electron low energies, impact excitation of electrons from the valence band is not effective because to satisfy the laws of energy and momentum conservation, E_p should be higher than $2E_g$ (the exact threshold value of E_p depends on the semiconductor band structure). The secondary electrons in this case are predominantly the primaries that escaped into the vacuum after losing their energy from optical phonon $\hbar\omega_{opt}$ scattering inside the crystal. The fine structure seen in figure 22(a) is discussed in the next section.

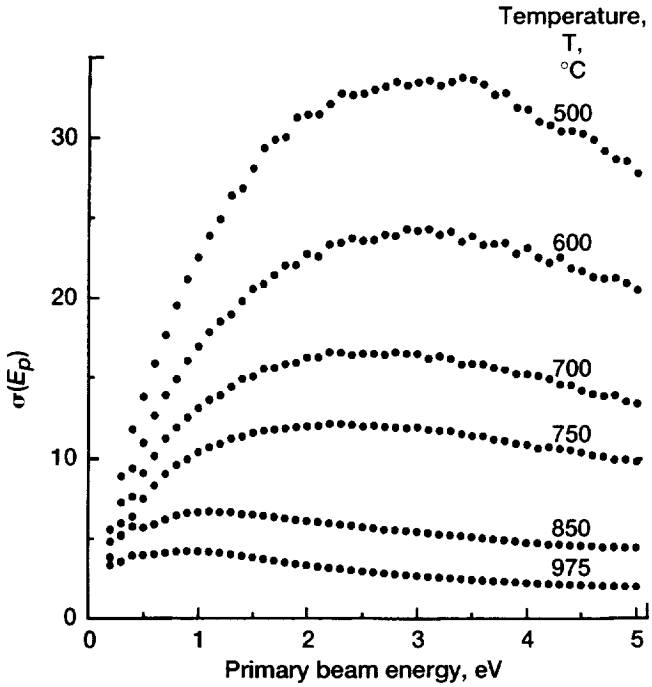

Figure 21.—Secondary electron yield $\sigma(E_p)$ after sample heating at various temperatures.

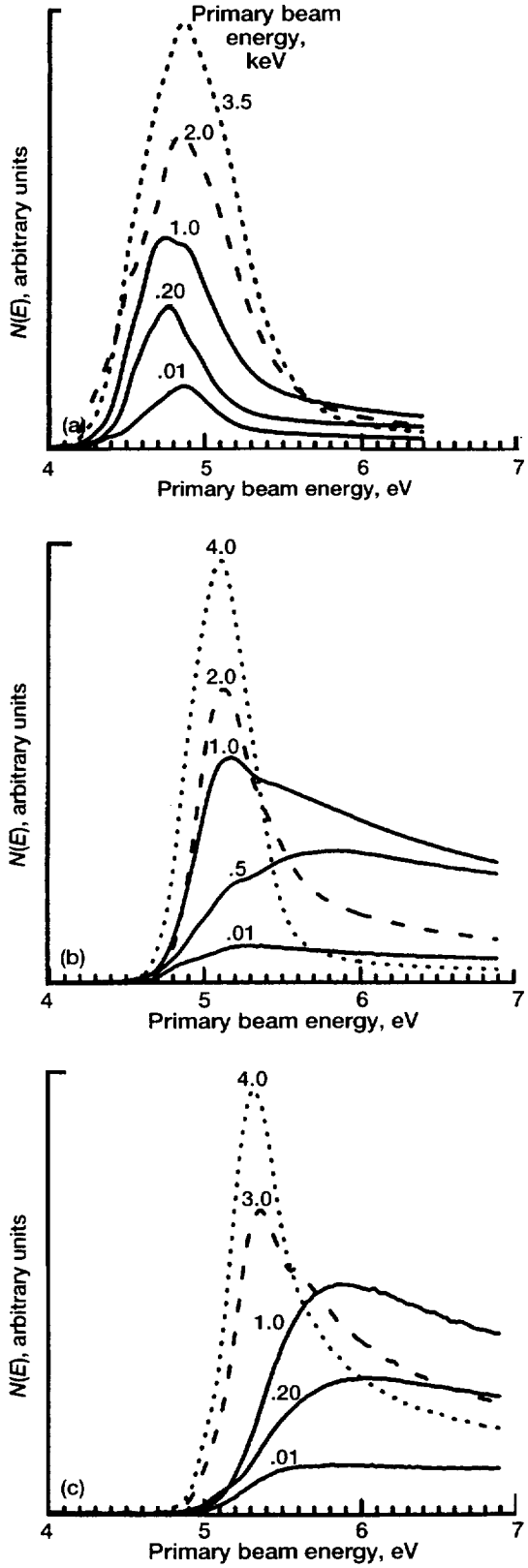

Figure 22.—Spectra of secondary electron energy distribution $N(E)$ for surfaces with various secondary electron emissions σ at several primary beam energies. (a) $\sigma = 35$. (b) $\sigma = 8$. (c) $\sigma = 4$.

The reduction in σ and the hydrogen coverage resulted in the emergence of some critical value of the primary electron energy E_p^c above which the NEA peak was observed in the energy spectrum of the secondary electrons. As seen from figures 22 (b) and (c), the lower the value of σ_{max}, the higher the magnitude of E_p^c.

Figure 23 shows the dependence of E_p^c on σ_{max}, which was determined as the value of E_p at which the NEA peak appears above the background. In the range of σ_{max} from 35 to 12, the NEA peak was observed at all primary energies used in our experiments, and the reported minimum value of $E_p = 10$ eV is shown in the plot as E_p^c for this coverage. At lower hydrogen coverage ($\sigma_{max} < 12$), E_p^c grows sharply and reaches 3 keV at $\sigma_{max} = 4$.

These experimental data are consistent with the demonstration that the type of NEA changes with hydrogen desorption from the diamond surface. It was suggested earlier (ref. 30) that after rehydrogenation, diamond exhibits downward band bending at the surface, thus having true NEA (fig. 20(b)). This model agrees with our observation of the NEA peak at very low primary electron energies on the completely rehydrogenated diamond surface. Indeed, at $E_p \leq 100$ eV, the penetration depth of the primary electrons l_p is only several interatomic distances (ref. 43); therefore, the existence of even a very low potential surface barrier would prevent the low-energy secondary electrons from escaping the solid. The critical height of the barrier can be estimated as $\chi_c \approx \varphi_{BB}\, l_p / L_{BB}$, where φ_{BB} is the band bending and L_{BB} is the length of the depletion layer (fig. 20(a)). At $\chi > \chi_c$, the electrons accumulated at the bottom of the conduction band within l_p of the surface cannot escape the crystal. For our highly doped CVD films ($N_A \approx 10^{18}$ to 10^{19} cm^{-3}), the

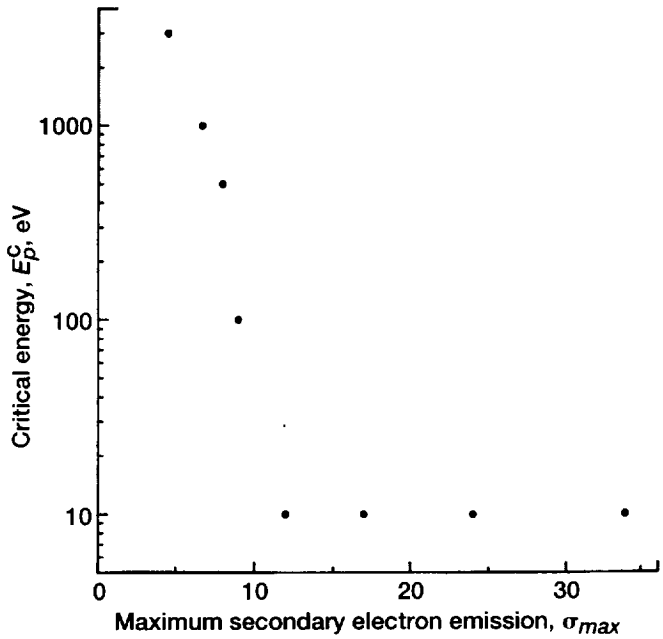

Figure 23.—Dependence of critical energy E_p^c on maximum secondary electron emission.

Fermi level position can be estimated at 0.3 to 0.4 eV above the top of the valence band in the bulk. In the case of the true NEA, the onset of the low-energy peak corresponds to the bottom of the conduction band at the surface and, as follows from figure 22, is equal to 4.3 eV. Then, using the value of 5.5 eV for the diamond band gap, we obtain $\varphi_{BB} \approx 1$ eV and $L_{BB} = (\varphi_{BB} \kappa/2\pi e N_A)^{1/2} \approx 100$ to 300 Å (where κ is the dielectric permeability of diamond). At $l_p \approx 10$ Å, the potential barrier $\chi_c \approx 0.03$ to 0.1 eV. Therefore, from the data presented in figure 22, we can conclude that for the diamond surface saturated with hydrogen, χ is at least about kT at room temperature and is probably negative.

The fact that there is a critical potential E_p^c for a surface with partially desorbed hydrogen indicates that the true affinity becomes positive, and the total (effective) NEA properties of the surface are now determined by the difference between the affinity and the band-bending potential. In this case, the NEA peak can be observed only when the penetration depth of the primary electrons is larger than a critical depth $l_c \approx \chi_c L_{BB}/\varphi_{BB}$ (fig. 20(a)). On the other hand, if $l_p \leq l_c$, the low-energy secondary electrons are captured by the surface potential and cannot escape the surface. It is well known (ref. 43) that l_p increases with the increase in the primary electron energy and, as it is clear from figure 20, the increase in χ should result in the shift of E_p^c to higher values. The capture of the low-energy secondary electrons by the surface can also be responsible for enhancing the low-energy peak intensity relative to the rest of the energy distribution curve that is observed in the range $E_p > E_p^c$ (see fig. 18).

In the effective NEA model, the onset of the NEA peak corresponds to the vacuum level and also has to move to higher energies. This agrees with the experimental data shown in figure 22. It can be seen that the NEA peak onset shifts to higher energy by approximately 0.6 eV when σ_{max} decreases from 35 to 4. The shift of the onset can be a consequence of both the increase in χ and the change in band bending. If we assume that all the shift is due to the change in χ and that for the surface saturated with hydrogen, $\chi \leq 0$, we can estimate for the surface with $\sigma_{max} = 4$ the upper limit for $l_c \approx 0.6 L_{BB} \approx 100$ Å, which is close to the value of l_p for electrons with energy equal to 3 keV (ref. 43). Therefore, we can conclude that the origin of the diamond surface NEA can change depending on the extent of the surface hydrogen coverage.

Fine Structure in Secondary Electron Emission Peak of Diamond with NEA Surface

It can be seen from figures 16 and 17 that FWHM of the low-energy peak is much larger than kT. Approximately the same NEA peak width has been observed in all photoemission measurements independent of the crystal orientation of the surface when samples were irradiated with photons whose energies significantly exceeded the diamond band gap (refs. 3, 4, 20, 29, and 30). It is therefore likely that the peak width is determined by the energy distribution of electrons inside the crystal rather than by the surface potential fluctuations (ref. 3). In this case, the low-energy peak of the secondary electrons should have features reflecting the energy structure of the bottom of the conduction band. A detailed study of the fine structure of this peak can contain essential information about the conduction band and mechanisms of the SEE process (refs. 44 and 45).

Diamond is a semiconductor with an indirect band gap. The two lowest energy minimums in the conduction band (absolute D_c minimum and X_c minimum) are located near the boundary of the Brillouin zone along the (100) direction (ref. 1). When the secondary electrons escape into the vacuum across a perfect surface, the component of the electron wave vector parallel to the surface $k_{||}$ and the electron energy should be conserved (ref. 41). The values of the crystal wave vector of electrons that occupy D_c and X_c minimums are close to the value of the reverse lattice constant. In the case of the (111) surface, $k_{||}$ values for the electrons in these minimums are so large that for a reasonable value of NEA, it is impossible to satisfy the laws of conservation of energy and momentum for the low-energy electrons escaping into the vacuum (ref. 41). The situation at the (100) surface is very different and is much more favorable for the emission of the secondary electrons into the vacuum. Electrons from two of the six D_c or X_c valleys located along the (100) direction, which is perpendicular to the (100) surface, have the $k_{||}$ component of the crystal wave vector equal to 0, so the conservation laws are easily satisfied for electrons escaping from these valleys. However, the measurements show that the intensity and angular distribution of the emitted secondary electrons depend very little on the surface orientation (refs. 3, 4, 20, 29, and 30), which indicates that the escape mechanism is more complicated and can include an additional interaction with the surface to satisfy the laws of conservation (ref. 30). This interaction would smear the measured energy distribution of secondary electrons and would impede the observation of a structure in the low-energy peak of secondary electrons from the (111) surface. It seems more conceivable to find fine features in the spectrum of secondary electrons from the (100) surface because a significant portion of these electrons can leave the crystal without any additional surface interaction.

This report describes the first observation of the fine structure in the low-energy electron peak of SEE from single-crystal diamond with an NEA (100) surface and from as-received polycrystalline CVD diamond films with surfaces that contain multitudes of (100) and (111) microcrystals.

Figures 24 and 25 show the low-energy portion of the secondary electron spectra for the (100) diamond surface and for an as-received CVD diamond film, respectively, as a function of the primary energy E_p monitored at a target potential $V_t = -1.5$ V. It can be seen that the important feature these spectra have in common is the existence of the prominent fine structure in the low-energy NEA peak consisting of four maximums. We were unable to observe a pronounced structure in the

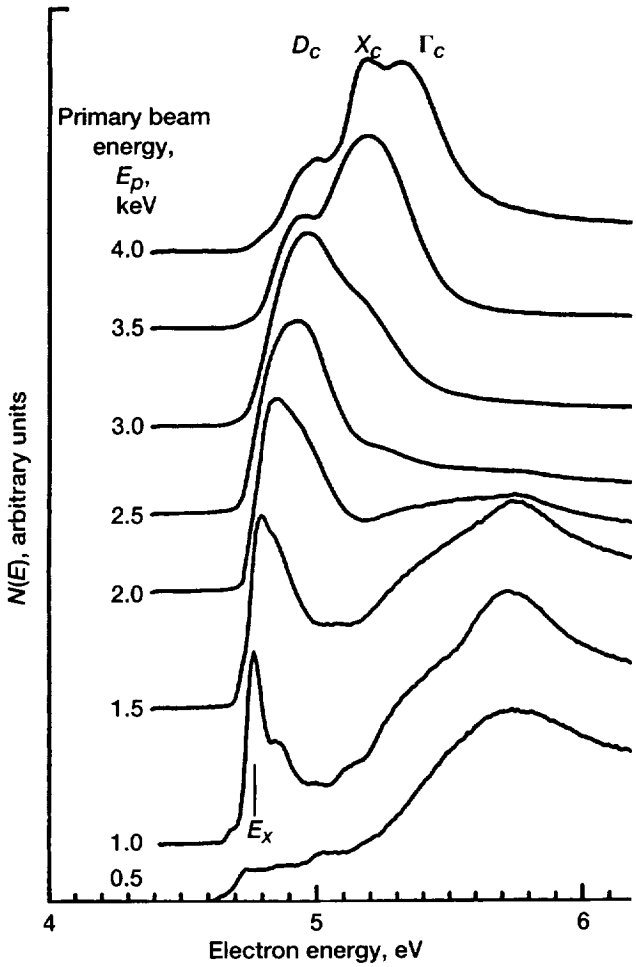

Figure 24.—Fine structure in low-energy portion of secondary electron energy distribution at V_t of −1.5 V and various E_p for (100) surface of single-crystal diamond.

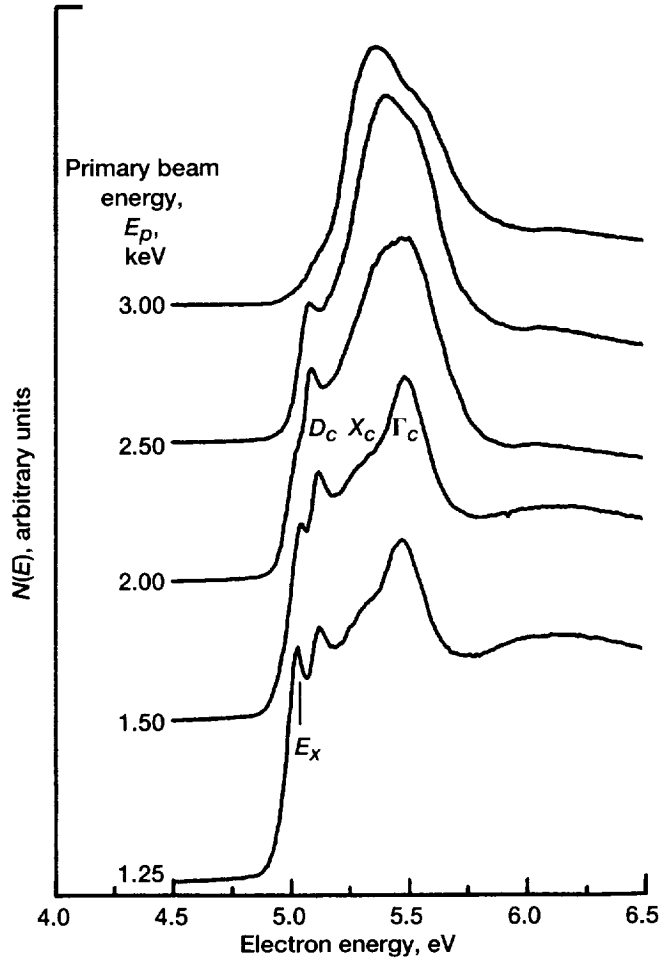

Figure 25.—Fine structure in low-energy portion of secondary electron energy distribution at V_t of −1.5 V and various primary beam electron energies E_p for CVD diamond film.

low-energy peak of secondary electrons emitted from the (111) surface.

It would appear reasonable that the newly found maximums reflect the energy structure of the bottom of the conduction band. Following the existing calculations of the diamond band structure (refs. 46 to 49) and the data obtained from photoemission measurements (ref. 50), we can attribute the fine structure maximums labeled D_c and Γ_c in figures 24 and 25 to the absolute minimum of the conduction band D_c and to the minimum in the center of the Brillouin zone Γ_c, respectively. From our data, the difference $\left(E_\Gamma - E_{D_C}\right)$ found is equal to 0.45 ± 0.05 eV as compared with 0.5 eV obtained from photoemission measurements by Himpsel, Van der Veen, and Eastman (ref. 50). The maximum X_c between them is probably associated with the X-minimum of the conduction band. Different theoretical calculations give a great variance in its energy position relative to the Γ minimum (refs. 46 to 50) with the latest calculations (ref. 46) giving the position of the X-minimum between the D_c and Γ_c minimums. As it follows from our data, $E_{\Gamma_c} - E_{X_c} = 0.25 \pm 0.05$ eV.

The most noticeable feature of the measured electron spectra is the narrow maximum labeled E_X located approximately 0.09 eV below the D_c feature. This energy is close to the exciton binding energy in diamond, which is equal to $E_{ex} = 0.08$ eV (ref. 51). The mechanism of the exciton-assisted electron emission in the photoemission process was suggested in reference 30 and should be similar to the role of the excitons in the SEE. The excitons are formed in the diamond as a result of the electron-hole Coulomb interaction during the cooling of the "hot" secondary electrons. The excitons drift to the surface and break up in the surface electric field, and the electrons are emitted into the vacuum.

Figure 26 illustrates this effect for the exciton with $m_h >> m_e$ for the single-crystal diamond surface with the true NEA. In our semi-insular crystals, the width of the depletion layer $L_{BB} \approx 1$ μm and the penetration depth of the primary electrons

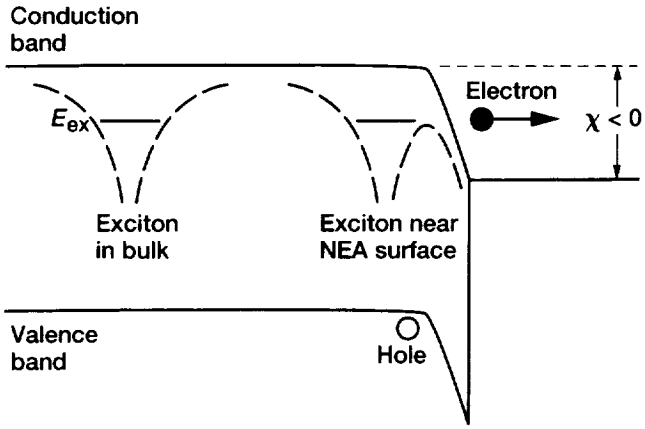

Figure 26.—Near-surface bands and exciton mechanism of SEE for diamond with true negative electron affinity at $l_p << L_{BB}$ and $m_h >> m_e$. E_{ex}, exciton binding energy.

$l_p << L_{BB}$. Therefore, within l_p below the surface, the diamond energy bands can be considered "flat." In this case, the electric field necessary to "ionize" the exciton is formed by a surface dipole (ref. 52) whose depth does not exceed 1 to 2 interatomic distances. Even for $|\chi| \approx 0.1$ eV, the electric field is greater than 10^6 V/cm. The electric field E_i that is necessary to break up an exciton can be estimated as $E_i \approx E_{ex}/(er_\hbar)$, where $r_\hbar$ is the Bohr radius of the exciton. In diamond, $r_\hbar$ = 15Å, E_{ex} = 0.08 eV (refs. 51 and 53), and $E_i \approx 5\times10^5$ V·cm^{-1}; therefore, the surface electric field is high enough to break up the exciton. Because the width of the surface dipole is smaller than the Bohr radius and the final state of the exciton hole after the breakup should be at the top of the valence band (fig. 26), the exciton breakup in the surface field is expected to yield a sharp maximum in the secondary electron spectrum.

The other favorable situation for observation of the exciton mechanism in SEE exists in the highly doped diamond CVD films when $l_p > L_{BB}$ and $r_\hbar \geq L_{BB}$. In this case, the secondary emission occurs also from the flat band area located below the depletion layer. As seen in figure 24, the absolute energy of the exciton peak for the CVD film almost exactly corresponds to the exciton energy level in the diamond bulk. Indeed, using $E_F \approx 0.4$ eV for the position of the Fermi level above the valence band (see the previous section), E_g = 5.5 eV and $E_{ex} \approx 0.1$ eV, we obtain for the peak energy the value of 5.0 eV above the Fermi level, which we observed experimentally. From the estimates made in the previous section, for our sample, $E_i = 2\varphi_{BB}/L_{BB} \approx 2\times10^6$ V·cm^{-1} at $L_{BB} \approx 100$ Å and $\varphi_{BB} \approx 1$ eV, which is enough to break up the excitons near the surface. We should also mention that in doped semiconductors, the excitons can be created only if the screening length is larger than the Bohr radius (ref. 54). At high carrier concentrations in our CVD samples, the regular theory of screening does not apply (ref. 55), and the screening radius may be estimated as equal to an average interparticle distance $r_{scr} \approx p^{-1/3}$, where $p \approx N_A$ is the hole concentration in the valence band. For the diamond films, $r_{scr} \geq 3\, r_\hbar$ allows the formation of the excitons.

As seen in figures 24 and 25, the exciton maximum is observable in the primary electron energy range of 0.5 to 2.5 keV and vanishes at higher electron energies. With E_p, the intensities of other maximums also change, with lower energy maximums reaching their highest intensity at a lower E_p. The increase in energy delivered to the crystal by the primary electrons increases the average energy of nonequilibrium electrons inside the crystal whereas the energy relaxation time τ_e remains unchanged. This process should result in a shift of the energy distribution of the secondary electrons towards the higher energies. Consequently, the probability of exciton creation should decline when the average electron energy becomes higher than the exciton binding energy.

The FWHM of each peak of the fine structure can be estimated from figures 24 and 25 to range from 0.15 to 0.3 eV. These widths are probably determined (besides the energy resolution of the analyzer) by the nonequilibrium distribution of low-energy electrons in the conduction band minimums. This nonequilibrium distribution is produced during the SEE process because the electron escape time τ_{esc} is smaller than the energy relaxation time τ_e, which is primarily determined by interaction with optical phonons. When the electron energy does not exceed the energy of a few optical phonons, the relaxation time can be estimated as $\tau_e \approx 10^{-12}$ to 10^{-13} s (ref. 56). At the penetration depth of the primary electrons in the crystal ($l_p \approx 100$ Å) and at the velocity of the low-energy secondary electrons, $v \approx 10^7$ cm·s^{-1} and $\tau_{esc} = l_p/v \leq 10^{-13}$ s. The condition $\tau_{esc} \leq \tau_e$ is fulfilled for all electrons contributing to the low-energy peaks that have an FWHM approximately equal to one or two times the energy of an optical phonon in diamond ($\hbar\omega_{opt}$ = 0.163 eV) (ref. 1). The relaxation time of electrons with energies less than $\hbar\omega_{opt}$ is even longer than 10^{-12} s. Therefore, we can expect that the FWHM of the energy distribution of secondary electrons in the conduction band minimums would be of the order of the energy of an optical phonon, as it was observed experimentally.

As it follows from the previous discussion, observation of the fine structure in the low-energy peak of the secondary electrons is possible only if certain conditions are satisfied, the most important being the "flat band" for the actual region under the surface from which the secondary electrons are emitted. The voltage drop due to band bending across this region should not exceed ≈ 0.1 V. This condition can be satisfied if $L_{BB} >> l_p$ (for a semi-insular crystal) or if $L_{BB} < l_p$ (for heavily doped diamond when emission occurs mainly from the region below the depletion layer). When the flat band condition is not satisfied, the fine structure can be broadened by the near-surface electric field. The other cause of broadening of the fine structure can be fluctuations of the surface charge, which creates band bending. Corresponding voltage variations inside the emission region should also be less than 0.1 eV in order to observe the fine structure.

Conclusions

Carbon Auger spectra of hydrogenated diamond surfaces were studied by using secondary electron emission spectroscopy (SEE). The findings were that the energy and shape of the Auger peak are dependent on the extent of surface hydrogen coverage. For both the single-crystal diamond and the chemical vapor-deposited (CVD) diamond films, we observed a shift in the AES carbon peak towards higher energies concomitant with an increase in the peak full width at half maximum (FWHM) when the hydrogen coverage of the diamond surfaces was diminished.

A theoretical model of Auger spectra for hydrogenated diamond surfaces was developed. The experimentally observed changes in the carbon Auger line shape were shown to be related to the redistribution of the valence-band local density of states caused by hydrogen desorption from the surface. One-electron calculations of Auger spectra of the diamond (111) and (100) surfaces having various hydrogen coverages were performed. The calculations were based on self-consistent wave functions and matrix elements calculated in the framework of the local density approximation and the self-consistent, linear, muffin-tin orbital method with static core-hole effects taken into account. The major features of the experimental spectra were qualitatively explained.

The SEE spectroscopy method was used to investigate the negative electron affinity (NEA) effect. We obtained direct proof of a strong NEA on the surface of CVD polycrystalline diamond films terminated with hydrogen. The effect appeared as a strong peak at the low-energy portion of the electron energy distribution.

The existence of the NEA peak in the energy spectrum of the secondary electrons for the partially hydrogenated diamond surface depends on the primary electron energy. There is a critical value of this energy at which the NEA peak appears in the spectrum. This critical energy increases sharply as hydrogen coverage of the diamond surface declines. This effect was explained by the change in NEA type from true for a fully hydrogenated surface to effective for a partially hydrogenated surface.

The fine structure in the SEE spectrum of the single-crystal diamond surface with NEA was observed for the first time and was demonstrated to be related to the electron energy structure of the crystal's conduction band. Spectroscopic proof of the existence of the SEE exciton mechanism was also obtained.

Glenn Research Center
National Aeronautics and Space Administration
Cleveland, Ohio, March 9, 1999.

References

1. Pan, L.S.; and Kania, D.R., eds.: Diamond: Electronic Properties and Applications. Kluwer Academic Publisher, Boston, MA, 1995.
2. Geis, M.W., et al.: IEEE Electron Device Lett., vol. 12, 1991, pp. 456–459.
3. Himpsel, F.J., et al.: Quantum Photoyield of Diamond (111): A Stable Negative-Affinity Emitter. Phys. Rev. B Conden. Matt., vol. 20, no. 2, 1979, pp. 624–627.
4. Van der Weide, J., et al.: Negative-Electron-Affinity Effects on the Diamond (100) Surface. Phys. Rev. B Conden. Matt., vol. 50, no. 8, 1994, pp. 5803–5806.
5. Mearini, G.T.; Krainsky, I.L.; and Dayton, J.A., Jr.: Investigation of Diamond Films for Electronic Devices. Surf. Interface Anal., vol. 21, no. 2, 1994, pp. 138–143.
6. Mearini, G.T., et al.: Fabrication of an Electron Multiplier Utilizing Diamond Films. Thin Sol. Fi., vol. 253, nos. 1 and 2, 1994, pp. 151–156.
7. Mearini, G.T., et al.: Stable Secondary Electron Emission From Chemical Vapor Deposited Diamond Films Coated With Alkali-Halides. Appl. Phys. Lett. (NASA CR–203599), vol. 66, no. 2, 1995, pp. 242–244.
8. Pepper, S.V.: Electron Spectroscopy of the Diamond Surface. Appl. Phys. Lett., vol. 38, 1981, pp. 344–346.
9. Jennison, D.R.: Energy-Band Theory of Auger Line Shapes: Silicon L_2, 3/VV and Lithium KVV. Phys. Rev. B Sol. State, vol. 18, no. 12, 1978, pp. 6865–6871.
10. Krainsky, I.L., et al.: Auger Electron Spectroscopy of the CVD Diamond Surface Under Electron Exposure. Diamond for Electronic Applications, MRS Symposium Proceedings, vol. 416, Materials Research Society, Pittsburgh, PA, 1996, pp. 431–435.
11. Krainsky, I.L., et al.: Auger Electron Spectroscopy of the Hydrogen Terminated Chemical Vapor Deposited Diamond Surface. Appl. Phys. Lett., vol. 68, no. 14, 1996, pp. 2017–2019.
12. Krainsky, I.L., et al.: Auger Spectroscopy of Hydrogenated Diamond Surfaces. Phys. Rev. B (NASA CR–97–207888), vol. 56, no. 20, Nov. 1997.
13. Krainsky, I.L., et al.: Diamond Materials. Proceedings of the Fifth Electrochemical Society, 1997, pp. 224–235.
14. Krainsky, I.L., et al.: Negative-Electron-Affinity Effect on the Surface of Chemical-Vapor-Deposited Diamond Polycrystalline Films. Phys. Rev. B, vol. 53, no. 12, 1996, pp. R7650–R7653.
15. Krainsky, I.L.; Asnin, V.M.; and Dayton, J.A., Jr.: Secondary Electron Emission From Chemical Vapor Deposited Diamond Films With Negative Electron Affinity. App. Surf. Sci., vol. 111, 1997, pp. 265–269.
16. Asnin, V.M.; and Krainsky, I.L.: Fine Structure in the Secondary Electron Emission Peak for CVD Diamond Films With Negative Electron Affinity. Proceedings of the 9th International Vacuum Microelectronics Conference, 1996, IEEE, New York, NY, pp. 354–357.
17. Krainsky, I.L., et al.: Auger Spectroscopy of Hydrogenated Diamond Surfaces. Phys. Rev. B, vol. 56, no. 20, 1997, pp. 529–534.
18. Asnin, V.M.; and Krainsky, I.L.: Negative Electron Affinity Mechanism for Diamond Surfaces. Appl. Phys. Lett., vol. 72, no. 20, 1998, pp. 2574–2576.
19. Wilks, J.; and Wilks, E.: Properties and Applications of Diamond. Butterworth-Heinmann, Oxford, England, 1991.
20. Pate, B.B.: The Diamond Surface Atomic and Electronic Structure. Surf. Sci., vol. 165, no. 83, 1986, pp. 83–142.
21. Bronshtein, I.M.; and Fraiman, B.S.: Secondary Electron Emission. Nauka, Moscow, 1969.
22. Oelhafen, P.; and Freeouf, J.L.: Accurate Spectrometer Calibration in Electron Spectroscopy. J. Vac. Sci. Technol. A, vol. 1, no. 1, 1983, pp. 96–97.
23. Johnson, J.B.: Secondary Electron Emission From Targets of Barium-Strontium Oxide. Phys. Rev., vol. 73, no. 9, 1948, pp. 1058–1073.
24. Krainsky, I.L.; and Lesny, G.G.: Simple Device for Monitoring Secondary Electron Emission of Materials in the Pulse Mode. J. Rev. Sci. Inst., vol. 69, no. 4, 1998, pp. 1916–1917.

25. Feibelman, P.J.; McGuire, E.J.; and Pandey, K.C.: Tight-Binding Calculation of a Core-Valence-Valence Auger Line Shape: Si (111). Phys. Rev. Lett., vol. 36, no. 19, 1976, pp. 1154–1157.
26. Feibelman, P.J.; McGuire, E.J.; and Pandey, K.C.: Theory of Valence-Band Auger Line Shapes: Ideal Si (111), (100), and (110). Phys. Rev. B Sol. State, vol. 15, no. 4, 1977, pp. 2202–2216.
27. Feibelman, P.J.; McGuire, E.J.: Valence Band Auger Line Shapes for Si Surfaces: Simplified Theory and Corrected Numerical Results. Phys. Rev. B Sol. State, vol. 17, no. 2, 1978, pp. 690–698.
28. Weightman, P.: X-Ray Excited Auger and Photoelectron Spectroscopy. Rep. Prog. Phys., vol. 45, 1982, pp. 753-814.
29. Pate, B.B., et al.: Electronic Structure of the Diamond (111) 1×1 Surface: Valence-Band Structure, Band Bending, and Band Gap States. J. Vac. Sci. Technol., vol. 17, no. 5, 1980, pp. 1087–1093.
30. Bandis, C.; and Pate, B.B.: Photoelectric Emission From Negative-Electron-Affinity Diamond (111) Surfaces: Exciton Breakup Versus Conduction-Band Emission. Phys. Rev. B Conden. Matt., vol. 52, no. 16, 1995, pp. 12056–12071.
31. Cini, M.: Two Hole Resonances in the XVV Auger Spectra of Solids. Solid State Commun., vol. 24, no. 9, 1977, pp. 681–684.
32. Cini, M.: Theory of Auger Line Shapes of Solids. J. Phys. Conden. Matt., vol. 1, suppl. B, 1989, pp. 55–61.
33. Houston, J.E., et al.: Relationship Between the Auger Line Shape and the Electronic Properties of Graphite. Phys. Rev. B Conden. Matt., vol. 34, no. 2, 1986, pp. 1215–1216.
34. Kovarik, P.; Bourdon, E.B.D.; and Prince, R.H.: Auger Electron Spectroscopy of Laser Deposited a-C, a-C:H, Microcrystalline Diamond. J. Vac. Sci. Technol. A, vol. 12, no. 4, 1994, pp. 1496–1500.
35. Hohenberg, P.; and Kohn, W.: Inhomogeneous Electron Gas. Phys. Rev., vol. 136, no. 3, 1964, pp. B864–B871.
36. Kohn, W.; and Sham, L.J.: Self-Consistent Equations Including Exchange and Correlation Effects. Phys. Rev., vol. 140, no. 4A, 1965, pp. A1133–A1138.
37. Almbladh, C.-O.; Morales, A.L.; and Grossmann, G.: Theory of Auger Core-Valence-Valence Processes in Simple Metals: I. Total Yields and Core-Level Lifetime Widths. Phys. Rev. B Conden. Matt., vol. 39, no. 6, 1989, pp. 3489–3502.
38. Almbladh, C.-O.; and Morales, A.L.: Theory of Auger Core-Valence-Valence Processes in Simple Metals: II. Dynamical and Surface Effects on Auger Line Shapes. Phys. Rev. B Conden. Matt., vol. 39, no. 6, 1989, pp. 3503–3516.
39. Slater, J.C.: The Self-Consistent Field for Molecules and Solids, Vol. 4, McGraw-Hill, New York, NY, 1974.
40. Andersen, O.K.; Jepsen, O.; and Sob, M.: Electronic Band Structure and its Applications, M. Yussouff, ed., Springer-Verlag, Berlin, Germany, 1987.
41. Bell, R.L.: Negative Electron Affinity Devices. Clarendon Press, Oxford, England, 1973.
42. Shih, A., et al.: Secondary Electron Emission From Diamond Surfaces. J. Appl. Phys., vol. 82, no. 4, 1997, pp. 1860–1867.
43. Lindau, I.; and Spicer, W.E.: The Probing Depth in Photoemission and Auger-Electron Spectroscopy. J. Electron. Spectrosc. Relat. Phenom., vol. 3, no. 5, 1974, pp. 409–413.
44. James, L.W.; and Moll, J.L.: Transport Properties of GaAs Obtained From Photoemission Measurements. Phys. Rev., vol. 183, no. 3, 1969, pp. 740–753.
45. Aspnes, D.E.: GaAs Lower Conduction-Band Minima: Ordering and Properties. Phys. Rev. B, vol. 14, no. 12, 1976, pp. 5331–5343.
46. Fong, C.Y.; and Klein, B.R.: Electronic and Vibrational Properties of Bulk Diamond. Diamond-Electronic Properties and Applications. Kluwer Academic Publishers, Boston, MA, 1995, pp. 1–29.
47. Painter, G.S.; Ellis, D.E.; and Lubinsky, A.R.: Phys. Rev. B Sol. State, vol. 4, no. 10, 1971, pp. 3610–3622.
48. Zunger, A.; and Freeman, A.J.: Phys. Rev. B Sol. State, vol. 15, no. 10, 1977, pp. 5049–5065.
49. Ihm, J.; Louie, S.G.; and Cohen, M.L.: Phys. Rev. B Sol. State, vol. 17, no. 2, 1978, pp. 769–770.
50. Himpsel, F.J.; Van der Veen, J.F.; and Eastman, D.E.: Experimental Bulk Energy Bands for Diamond Using $h\nu$-Dependent Photoemission. Phys. Rev. B, vol. 22, no. 4, 1980, pp. 1967–1971.
51. Dean, P.J.; Lightowlers, E.C.; and Wight, D.R.: Phys. Rev., vol. 140, no. 1A, 1965, pp. A352–A368.
52. Pate, B.B., et al.: Electronic Structure of the Diamond (111) 1×1 Surface: Valence-Band Structure, Band Bending, and Band Gap States. J. Vac. Sci. Technol., vol. 17, no. 5, 1980, pp. 1087–1093.
53. Davies, G.: Cathodoluminescence. Properties of Diamond, J.E. Field, ed., Academic Press, London, England, 1979, pp. 165–181.
54. Asnin, V.M.; and Rogachev, A.A.: Phys. Stat. Sol., vol. 20, 1967, pp. 755–757.
55. Pines, D.: Elementary Excitations in Solids. W.A. Benjamin, Inc., New York, NY, 1963.
56. Conwell, E.M.: High Field Transport in Semiconductors. Academic Press, New York, NY, 1967.

REPORT DOCUMENTATION PAGE

Form Approved
OMB No. 0704-0188

1. AGENCY USE ONLY (*Leave blank*)	2. REPORT DATE	3. REPORT TYPE AND DATES COVERED
	October 1999	Technical Paper

4. TITLE AND SUBTITLE

Secondary Electron Emission Spectroscopy of Diamond Surfaces

5. FUNDING NUMBERS

WU–632–50–5D–00

6. AUTHOR(S)

Isay L. Krainsky, Vladimir M. Asnin, and Andre G. Petukhov

7. PERFORMING ORGANIZATION NAME(S) AND ADDRESS(ES)

National Aeronautics and Space Administration
John H. Glenn Research Center at Lewis Field
Cleveland, Ohio 44135–3191

8. PERFORMING ORGANIZATION REPORT NUMBER

E–11357

9. SPONSORING/MONITORING AGENCY NAME(S) AND ADDRESS(ES)

National Aeronautics and Space Administration
Washington, DC 20546–0001

10. SPONSORING/MONITORING AGENCY REPORT NUMBER

NASA TP—1999-208692

11. SUPPLEMENTARY NOTES

Isay L. Krainsky and Vladimir M. Asnin, NASA Glenn Research Center; Andre G. Petukhov, Physics Department, South Dakota School of Mines and Technology, Rapid City, SD 57701-3995. Responsible person, Isay L. Krainsky, organization code 5620, (216) 433–3509.

12a. DISTRIBUTION/AVAILABILITY STATEMENT

Unclassified - Unlimited
Subject Category: 76 Distribution: Standard

This publication is available from the NASA Center for AeroSpace Information, (301) 621–0390.

12b. DISTRIBUTION CODE

13. ABSTRACT ***(Maximum 200 words)***

This report presents the results of the secondary electron emission spectroscopy study of hydrogenated diamond surfaces for single crystals and chemical vapor-deposited polycrystalline films. One-electron calculations of Auger spectra of diamond surfaces having various hydrogen coverages are presented, the major features of the experimental spectra are explained, and a theoretical model for Auger spectra of hydrogenated diamond surfaces is proposed. An energy shift and a change in the line shape of the carbon core-valence-valence (KVV) Auger spectra were observed for diamond surfaces after exposure to an electron beam or by annealing at temperatures higher than 950 °C. This change is related to the redistribution of the valence-band local density of states caused by hydrogen desorption from the surface. A strong negative electron affinity (NEA) effect, which appeared as a large, narrow peak in the low-energy portion of the spectrum of the secondary electron energy distribution, was also observed on the diamond surfaces. A fine structure in this peak, which was found for the first time, reflected the energy structure of the bottom of the conduction band. Further, the breakup of the bulk excitons at the surface during secondary electron emission was attributed to one of the features of this structure. The study demonstrated that the NEA type depends on the extent of hydrogen coverage of the diamond surface, changing from the true type for the completely hydrogenated surface to the effective type for the partially hydrogenated surface.

14. SUBJECT TERMS	15. NUMBER OF PAGES
Auger spectrum; Secondary electron emission; Diamond	24
	16. PRICE CODE: A03

17. SECURITY CLASSIFICATION OF REPORT	18. SECURITY CLASSIFICATION OF THIS PAGE	19. SECURITY CLASSIFICATION OF ABSTRACT	20. LIMITATION OF ABSTRACT
Unclassified	Unclassified	Unclassified	